FOREWORD

This report was prepared by the Fracture Research Laboratory of the Department of Theoretical and Applied Mechanics, University of Illinois under USAF Contract No. AF 33(616)-8177. The contract was initiated under Project No. 7351, "Metallic Materials," Task No. 735106, "Behavior of Metals." The work was administered under the direction of the Air Force Materials Laboratory, Research and Technology Division, K. D. Shimmin, project engineer.

This report covers work conducted from April 1961 to June 1963.

Helpful suggestions were contributed by Prof. T. J. Dolan, Head of the Department of Theoretical and Applied Mechanics, and Prof. J. Morrow.

The assistance of Mrs. Hazel Corray and Brian Gain in preparing the manuscript is gratefully acknowledged.

ABSTRACT

When a tubular specimen of copper is subjected to a small steady tension and alternating torsion at room temperature large axial strain increments accumulate on a cyclic basis. At relatively low values of axial stress a steady state cyclic strain accumulation is observed to develop. The strains and cyclic strain rates which are observed are many orders of magnitude greater than corresponding values obtained under conditions of standard static creep tests performed at the same peak effective stress. They are also many times larger than those obtained due to simple repetition of the effective stress in more conventional dynamic creep tests. The experiments reported herein were designed to produce an extreme case of cyclic creep wherein time and temperature dependence are minimized. The analysis of results includes a comparison with plasticity theory predictions as well as a parameteric description of minimum cyclic creep rate.

This technical documentary report has been reviewed and is approved.

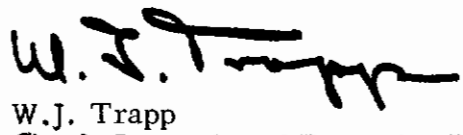

W.J. Trapp
Chief, Strength and Dynamics Branch
Metals and Ceramics Division
Air Force Materials Laboratory

TABLE OF CONTENTS

LIST OF ILLUSTRATIONS

Cyclic Strain Accumulation under Complex Multiaxial Loading

by

G.J. Moyar and G.M. Sinclair

Introduction

In 1909 Bairstow reported some careful observations of strain accumulation in axle steel under cyclic uniaxial stressing with positive mean stress. He reports; "the change in cyclical permanent set (width of hysteresis loop) is thus seen to have been accompanied by a change of length, and when the set had become constant, the rate of extension had also become constant and small but not zero" [1]. The study of this rate of extension or accumulation of axial strain has been the subject of a number of recent papers for elevated temperature [2] [3] [4] [5] as well as room temperature [6] [7] [8]. Other observations of remarkable strain accumulation at low temperatures have been cited in multiaxial non-proportional loading investigation [9] [10] [11]. When a tubular specimen of copper is subjected to steady tension and alternating torsion at room temperature, relatively large axial strain increments are observed which eventually develop into a steady state cyclic strain accumulation. These strains and cyclic strain rates are many orders of magnitude greater than the corresponding values obtained in standard creep tests performed at the same peak "effective" stress. They are also many times larger than those obtained due to simple repetition of the effective stress in more conventional dynamic creep tests [12].

Guidelines for the phenomenological description of cyclic strain accumulation and correlation of significant mechanical variables are not well established even for uniaxial loading. Current methods of analysis [13], involving integration of an equation of state over the loading path, apply primarily to elevated temperature behavior, that is, for temperatures greater than 1/2 the absolute melting point. Even in this case the correlation is very poor for non-proportional loading or changing stress ratios [14] [15]. For temperatures less than half the absolute melting point the interest has centered primarily on fatigue fracture rather than the accompanying deformation per se, although in certain circumstances such deformation may be appreciable. Perhaps the only related study of large scale cyclic plastic deformation is the plasticity analysis of incremental collapse of structures.

The experiments reported in this paper were designed to produce an extreme case of cyclic creep wherein time and temperature dependence are minimized. The

Manuscript released by the authors October 1963 for publication as an RTD Technical Report.

analysis of results includes a comparison to plasticity theory prediction as well as parametric description of minimum cyclic creep rate.

Test Program

A series of 20 cyclic tests on long specimens of annealed OFHC copper tubing were performed in which axial stress ranged from 2,000 to 11,000 psi and the range of alternating shear strain varied from 5.5×10^{-3} to 14.5×10^{-3}. Observations of extension, angle of twist, torque and diameter were recorded as a function of number of cycles. In addition to these tests a number of special multiaxial loading tests were performed.

Material

The OFHC copper tubing was certified by the manufacturer to be 99.97 copper by weight per cent. The average outside diameter was .3739 inch with a maximum variation of less than one per cent. The average wall thickness was .0303 inch with a maximum variation of 5 per cent. A true stress-strain curve is shown in Fig. 1. This curve was determined from tests of 6.375 inch lengths of tubing. The plot includes data points based on overall length change.

$$\left(\epsilon = \ln \frac{\ell}{\ell_o}\ ,\ \sigma = \frac{P}{A_o} \times \frac{\ell}{\ell_o}\right)$$

and minimum diameter

$$\left(\epsilon = 2 \times \ln \frac{D_o}{D}\ ,\ \sigma = \frac{P}{A} \times \frac{\ell}{\ell_o}\right)$$

Five tension tests were performed on sections of tubing picked at random from the 20 tubes used in the cyclic tests. Variations in load extension curves were small. A comparison to the annealed copper tubing used by Taylor and Quinney [16] in their classical experiments in 1931 is provided by the cross marks indicated up to 10 per cent strain.

Apparatus

A schematic of the apparatus is presented in Fig. 2. The long specimen (44 inches between grips) minimized the alignment difficulties and simplified strain measurement. The grips were similar in principle to those used by Taylor and Quinney. The upper grip was coupled to a spindle and pulley supported by a ball thrust bearing. Alternating angle of twist was applied to this pulley through cables

driven by a scotch yoke mechanism. The bottom grip was attached to flex-bars that were instrumented for recording of the torque transmitted through the specimen, so that support bearing friction did not influence the torque indication. Axial load was applied to the weight pan attached to the bottom grip. Axial extension was recorded on a separate chart via a simple mechanical linkage that magnified extension by approximately a factor of two.

Procedure

The cyclic frequency was 15 cycles per minute for all tests. This low speed was used to prevent pronounced heating of the specimen at the highest strain amplitude. After axial strain increments of approximately .023 inch per inch the machine was stopped (approximately one minute) and adjustment was made in axial load and amplitude of angle of twist to correct the current values of axial stress and shear strain to the original values. The corrections were made in accordance with

$$P = P_o \times \frac{\ell_o}{\ell} \quad \text{and} \quad \theta = \theta_o \times \left(\frac{\ell}{\ell_o}\right)^{3/2}$$

where uniform deformation and constant volume of specimen were assumed. Diameter measurements were taken periodically at three locations along the specimen. All specimens were tested to fracture.

Results

True axial strain accumulation for all tests is given in Figs. 3a through 3e. Those specimens experiencing a strain greater than approximately 20 per cent exhibited a localized dimensional instability. This may be seen by reference to a plot of diameter at various numbers of cycles against location along the specimen (see Figs. 4a through 4e). In these tests at the higher strain amplitudes and loads a noticeable drop in torque (5a through 5e) occurred at values of N corresponding to about 0.2 in/in strain. It should be noted that the maximum load in a simple tension test occurred at 0.3 in/in. strain; therefore, the instability in the complex multiaxial loading sets in before that which might be expected in an ordinary creep test. In general, excepting the data after the instability occurred, there was a cyclic hardening of shear stress after which a steady state value was maintained or a slight decrease was noted. Significantly, those specimens with the higher axial stress hardened to a greater peak value of shear stress than those specimens with the same shear strain amplitude but a lower axial stress. Corresponding to the

higher values of peak shear stress was a lower value of plastic range of shear strain, which is to be expected for tests at the same total shear strain range. It does appear that in these tests, which in most cases involve shear strain ranges large in comparison to the elastic shear strain range, that the shear stress-strain hysteresis loop adjusted to a configuration of maximum plastic work for the higher axial stresses.

After a minimum cyclic creep rate was reached, the total work per cycle performed by the machine in twisting the specimen was much greater than the work done on the specimen by the axial load. At the highest load the work done by the axial load was less than 2 per cent of the total work done on the specimen. For these reasons the work per cycle may be characterized simply by a work per cycle index, W, defined in this case to be the range of shear stress times the range of plastic shear strain. This affords a convenient index for comparison since the shape change in hysteresis loop could account for only a small variation in the ratio of total work per cycle under one condition to the work per cycle under another condition of loading.

The onset of dimensional instability in seven of the tests was taken as the end of accurate strain indication and "steady state cyclic creep". Note the instability is particularly pronounced in this case because once it occurs the rest of the specimen is virtually unloaded with respect to the angle of twist per unit length. Therefore the strain versus cycles curves are shown dotted beyond this region and the minimum cyclic creep rate is taken as the slope at this point. The work index per cycle as a function as a number of cycles is illustrated in Fig. 6 for typical specimens. Except for those tests with marked instabilities the work index reached a constant value. If an instability occurred the work index used in the following analysis was taken at the instability point which corresponded to the minimum cyclic creep rate. The significant test results are summarized in Table I.

Analysis

For the purposes of discussion the strain accumulation will be divided into three parts, initial deformation, transient strain, and steady state.

Initial Deformation

It is expected that existing plasticity theories would prove useful in prediction of initial strain on application of the first twist. Since the loading is quite non-proportional it is necessary to use one of the incremental theories. For the case of combined tension and torsion of a thin wall tube of isotropic hardening material the

incremental relations [17] specialize to

$$d\epsilon = \frac{\sigma}{\bar{\sigma}\ H}\ d\bar{\sigma} + \frac{d\sigma}{E} \tag{1}$$

and, for the conventional shear strain definition,

$$d\gamma = \frac{9\,\tau^2\ d\tau}{H'\,\bar{\sigma}^2} + \frac{d\tau}{G} \tag{2}$$

Where

$$\bar{\sigma} = (\sigma^2 + 3\tau^2)^{1/2} \tag{3}$$

and

$$H' = \frac{d\bar{\sigma}}{d\bar{\epsilon}_p} \tag{4}$$

$\bar{\sigma}$ is the effective stress and $\bar{\epsilon}_p$ the effective plastic strain,

$$\epsilon_p = (\epsilon_p^2 + \frac{\gamma_p^2}{3})^{1/2} \tag{5}$$

A frequently used non-linear hardening relation is

$$\bar{\epsilon}_p = (\frac{\bar{\sigma}}{\sigma_{p1}})^{1/n}$$

If this relation is adopted, then equation 1 may be integrated and the strain solved in terms of the effective stress $\bar{\sigma}_1$ at the end of the first twist application:

$$\epsilon = \frac{\sigma_o}{E} + (\frac{\sigma_o}{\sigma_{p1}})^{1/n} + \frac{\sigma_o}{(1-n)\,\sigma_{pl}^{1/n}} \left(\bar{\sigma}_1^{\frac{1-n}{n}} - \sigma_o^{\frac{1-n}{n}} \right) \tag{6}$$

Equation 2 must first be integrated to solve for the shear stress and hence the effective stress at the end of the first twist application. The general form of equation 2 is

$$dy = \frac{x^2\ dx}{(x^2+1)^{\frac{3n-1}{2n}}} \tag{7}$$

where

$$y = \frac{n\ \gamma_p}{\sqrt{3}\ (\frac{\sigma_o}{\sigma_{p1}})^{1/n}}$$

and

$$x = \sqrt{3}\ \frac{\tau}{\sigma_o}$$

which may be integrated explicitly for integral values on 1/n. n = 1/3 is a fair approximation of the slope of the stress-plastic strain curve over the entire range (see Fig. 7) and for purposes of illustration will be used here. After the integration of equation 7 the shear stress is determined in terms of the cubic equation:

$$\tau^3 + \frac{\sigma_{pl}^{\ 3}}{9G}\ \tau - \frac{\sigma_{pl}^{\ 3}\ \gamma_o}{9} = 0 \qquad (8)$$

The real root of this equation is

$$\tau = \frac{\sigma_{pl}\gamma_o}{18^{1/3}}\left\{\left(1 + \sqrt{1 + \frac{4\sigma_{pl}^{\ 3}}{243\ G^3\gamma_o^{\ 2}}}\right)^{1/3} + \left(1 - \sqrt{1 + \frac{4\sigma_{pl}^{\ 3}}{243\ G^3\gamma_o^{\ 2}}}\right)^{1/3}\right\} \qquad (9)$$

or to a high degree of accuracy

$$\tau = \frac{\sigma_{pl}\ \gamma_o^{\ 1/3}}{9^{1/3}} \qquad (10)$$

since

$$\frac{4\sigma_{pl}^{\ 3}}{243\ G^3\gamma_o^{\ 2}}$$

is very small for values used experimentally. Thus the initial axial strain in terms of the material parameters σ_{pl}, n and the load conditions σ_o and γ_o is

$$\epsilon_o = \frac{\sigma_o}{E} + \left(\frac{\sigma_o}{\sigma_{pl}}\right)^3 + \frac{9^{1/3}}{2}\ \frac{\sigma_o}{\sigma_{pl}}\ \gamma_o^{\ 2/3} \qquad (11)$$

Strains obtained from this equation correspond favorably with the actual strains observed (see Fig. 8). In general, the strains at high loads are underestimated and those at low loads overestimated.

Transient Strain

When the shear strain is reversed, additional axial strain would be expected from the plasticity analysis. This may be appreciated by reference to the one-

dimensional isotropic hardening model in Fig. 9. According to the theory an entirely elastic response will eventually occur, that is, the maximum shear stress will eventually equal $\gamma_o G$. Therefore the maximum axial strain that may be accumulated for an enforced shear strain amplitude is

$$\epsilon_{max} = \frac{\sigma_o}{E} + \left(\frac{\sigma_o}{\sigma_{pl}}\right)^3 + 4.5 \frac{\sigma_o}{(\sigma_{pl})^3} (G\gamma_o)^2 \qquad (12)$$

From a consideration of the cyclic twisting, the general relation between successive absolute magnitudes of shear stress at the end of m twist reversals may be expressed in the following equation:

$$\tau^3_{m+1} + \frac{\sigma_{pl}^3}{9G} \tau_{m+1} - 2\frac{\sigma_{pl}^3}{9} \gamma_o - \tau^3_m + \frac{\sigma_{pl}^3}{9G} \tau_m = 0 \qquad (13)$$

subject to the initial conditions on the first twist application given in equation (8).

A numerical or graphical reiterating procedure may be used to solve for successive values of shear stress amplitude. From equation (13) asymptotic approach to the limit can be verified:

$$\tau_m \longrightarrow \tau_{m+1} \longrightarrow G\gamma_o$$

As an example, the test conditions of specimen 18s would result in the strain vs number of cycles curve indicated in Fig. 10. The actual data fall appreciably below this in the transient region. That is, the actual process moves toward a stable configuration of energy dissipation and a corresponding cyclic axial creep rate, and not to a purely elastic response which necessitates a large shear stress value. On the other hand the theoretical result for alternating shear stress is entirely different. According to the isotropic hardening theory no further strain accumulation is possible. However, in actual fact considerable strain accumulation can occur [12]. Actual data from previous experiments in which alternating torque was applied to the tubular specimens are presented for comparison (Fig. 10). The value of shear stress amplitude attained in the enforced shear strain test at 965 cycles is nearly identical to the shear stress amplitude enforced in the test

selected for comparison. The corresponding rates of strain accumulation are also comparable. The inset diagram provides a comparison of the cyclic shear stress and strain behavior of the two specimens. These observations lend support to a statement by Benham: "It thus appears that there is a particular 'cyclic condition' for a metal that is achieved whatever the mode of cycling."[6] The idea of a "stabilized" shear stress-strain curve for cyclic loading is complicated somewhat by the observation of the influence of axial stress. These results for enforced shear strain, indicate that such a curve would be raised by an increase in axial stress. If these curves were valid for enforced shear stress conditions, then a test with a high value of axial stress would involve less hysteresis in the stable condition than in a corresponding test at the same shear stress range but with a low axial stress. A study of the stable cyclic condition under multiaxial loading thus presents possibilities not inherent in uniaxial loading. Such studies would be especially significant with respect to this research since it appears, in what follows, that one of the parameters most appropriately associated with the cyclic creep rate is the work per cycle.

A review of current plasticity theories [18] has indicated that none will successfully predict a steady state strain accumulation, although the kinematic hardening theories do predict a brief transient strain accumulation period. The fact that energy is dissipated in slip for alternating shear stress (in some sense a Bauschinger effect) limits the applicability of the plasticity theories. They do provide limits however for the observed strain values.

If the transient strain is determined by subtracting the initial strain at the end of the first twisting and the steady state strain (the slope indicated on the strain-number of cycles curve x number of cycles) a plot of log transient strain versus log number of cycles reveals a trend in the transient exponent. The slopes range from .247 to .477. In general, steeper slopes occur at the larger ranges of shear strain. (See Figs. 11a through 11e).

Meleka and Evershed [5] report values of transient creep exponents for both simple creep and combined fatigue-creep of OFHC copper at 752° F. Superimposed fatigue stressing was conducted at a frequency of 20 cps. Static transient creep was in accord with the Andrade β flow type (exponent = 1/3). However considerable emphasis was placed on the particular value of 2/3 reported for the combined fatigue creep test even though it is very questionable to ignore the influence of frequency or number of cycles over a given time period. A significant change

in frequency would most certainly influence the value reported.

Steady State Strain Accumulation

A serious limitation of the inviscid mechanics of solids idealizations is their inability to include, even qualitatively, a steady state cyclic strain accumulation. Therefore, a parametric description is warranted. The most satisfactory parameter for the specification of minimum cyclic creep rate appears to be the work per cycle index. From Fig. 12 a relation of the form

$$\Delta \epsilon_N = A W^B \tag{14}$$

appears justified. Coefficient A is a function of axial stress while B is nearly independent of axial stress. The correlation of minimum cyclic creep rate in terms of work per cycle and a directing stress, perhaps the largest mean value of principle stress acting over the cycle, would be a meaningful way to interpret results in various loading configurations.

It is tempting to consider the phenomenon as a mechanically activated creep process since in the limiting case ($\Delta \gamma$ approaches 0) ordinary creep conditions are encountered.

Fracture Observations

The predominant fracture mode was characterized by the propagation of a longitudinal crack along the tube axis and a final tearing transverse to the tube axis. Typical fractures are shown in the photograph of Fig. 13a.

At high values of axial stress a neck preceded fracture in some cases, as shown in Fig. 13b. Both instability necks and longitudinal cracks are shown in the specimen stopped prior to complete fracture at initial loading conditions:

stress = 7000 psi and range of shear strain = 9.2 inches per inch x 10^{-3}.

The preference for fatigue crack propagation along the tube axis may be due to the presence of a fibrous flaw structure oriented in the axial direction during the tube drawing operation. According to Backofen et al [19], this oriented flow structure in copper would not be removed by annealing.

The transition in failure mode from the fatigue "split" along the tube axis to the localized "neck" separation at the higher loads and shear strain ranges is similar in some respects to that observed by Benham under uniaxial load cycling.

He differentiates between the conventional fatigue fracture (no gross plastic distortion around the crack) and a "necked-out" fracture observed in the low cycle region accompanied by large cyclic creep rates.

Although the data are insufficient for an analyses of fracture criteria several observations appear to be justified. The range of plastic shear strain alone is not a satisfactory index for life prediction, nor is the plastic work per cycle alone. For any group of tests at the same enforced strain range the minimum plastic shear strain range was smallest for the test with the largest axial stress which in general exhibited a shorter life. An examination of Table I also reveals several pairs of tests in which the longer life is associated with the larger work per cycle index. Perhaps the most satisfactory criteria for engineering purposes would be one based on the plastic work per cycle modified for the axial or directing stress acting.

Special Initial Loading Tests

In order to examine more closely the influence of axial stress on the shear stress values for enforced shear strain, the machine was modified to apply monotonically increasing angle of twist to four specimens at the axial stress levels used in the cyclic tests. Angle of twist, extension and torque were recorded simultaneously. The shear stress-strain results are shown in Fig. 14. Initially the shear stress values are in accordance with usual prediction of plasticity theories, that is, the smaller shear stress corresponds to the larger axial stress. But the strain hardening is more pronounced for the higher axial stresses and the relationship is soon inverted for relatively small strains. It should be noted that the isotropic hardening theory for the unique case of $n = 1/3$ predicts that the shear stress-shear strain relation is independent of axial stress. Apparently this behavior is due to anisotropy which develops during straining.

In addition a pronounced cross effect similar in many respects to that reported by Parker and others [20] was observed on tension reloading. The initial loading process is presented in terms of effective stress and effective plastic strain in Fig. 15. The deviation from a unique effective stress and effective plastic strain curve is not surprising for such non-proportional loading. However, the effective stress strain curve on reloading in tension tends to a much higher level indicating very anisotropic hardening.

These two general observations, that is, the influence of the axial stress on the shear stress and the cross effect, are apparently at variance with the results

of Taylor and Quinney on similar copper tubing but under conditions of dead loading. In their tests a very large axial pre-strain was applied. For loading under various ratios of torque and axial load the yield values (determined by backward extrapolation of the flow stress curves) in terms of effective stress do not differ significantly from the stresses at the end of pre-strain. Also no inversion of the shear stress-strain curves is reported, although here the large pre-strain must be considered.

In any event it appears that experimental studies under mixed boundary conditions would provide data of considerable interest for the development of plasticity theories since there is indication of phenomena of more practical concern than local discontinuities at the loading point.

Conclusions and Recommendations

From room temperature tests of annealed copper tubing subjected to steady tension and alternating shear strain the following conclusions may be made.

1. Initial axial strain may be predicted with reasonable accuracy by isotropic hardening plasticity theory specialized for nonlinear hardening according to

$$\bar{\epsilon}_p = \left(\frac{\bar{\sigma}}{\sigma_{pl}}\right)^{\frac{1}{n}}$$

2. Transient strain accumulation would be predicted for conditions of enforced shear strain by isotropic hardening plasticity theory but not under conditions of enforced shear stress. Appreciable strain accumulation is actually observed under both loading conditions. True the plasticity theory only forms limits in this region of strain accumulation.

3. There is indication that a unique cyclic state is approached for either conditions of enforced shear stress or shear strain.

4. An increase in axial stress increases the maximum amplitude of shear stress for cyclic tests at the same enforced shear strain range.

5. Minimum cyclic creep rate appears to be described most effectively in terms of the plastic work per cycle and the directing stress.

6. Both fatigue type "splitting" of the tubes and creep type "necked" ruptures were observed. A plastic work per cycle criterion modified to include the influence of the axial stress may be applicable.

7. Pronounced dimensional instabilities were induced in the long specimens at the higher load and shear strain ranges. The instability developed after an axial strain of approximately .20.

8. In special initial loading tests, under constant tension and monotonically increasing shear strain, the hardening, with respect to shear stress, increases with an increase in axial stress. Tension reloading produces a large cross effect.

The major recommendation from this research is an extension of the correlation of plastic work and directing stress to minimum cyclic creep rate under other conditions of loading, including the limiting case of uniaxial loading under various mean stresses (Bairstow's, original test configuration). A complete study of the cyclic steady state approached for various initial loading conditions is necessary for purposes of estimating the steady state conditions including the minimum cyclic creep rate. Inclusion of frequency and temperature effects are a natural extension of these experiments.

References

1. L. Bairstow, "The Elastic Limits of Iron and Steel under Cyclical Variations of Stress," Philosophical Transactions of the Royal Society, Ser. A., Vol. 210. pp. 35-55 (1911).

2. B. J. Lazan, "Dynamic Creep and Rupture Properties of Temperature-Resistant Materials under Tensile Stress," American Society for Testing Materials, Proceedings, Vol. 49, pp. 757-787 (1949).

3. M. J. Manjoine, "Effect of Pulsating Loads on the Creep Characteristics of Aluminum Alloy 14S-T," American Society for Testing Materials, Proceedings Vol. 49, pp. 788-798 (1949).

4. A. J. Kennedy, "Effect of Fatigue Stresses on Creep and Recovery," International Conference on Fatigue of Metals, Inst. of Mech. Eng., London, ASME, Sept. 1956, p. 401.

5. A. H. Meleka and A. V. Evershed, "The Dependence of Creep Behavior on the Duration of a Superimposed Fatigue Stress," Journ. of Inst. of Metals, May 1960, pp. 411-414.

6. P. P. Benham, "Axial - Load and Strain-Cycling Fatigue of Copper at Low Endurance," J. Inst. Met. Vol. 89, p. 328, (1961).

7. C. P. Sullivan, "Repeated Tensile Loading of Iron and Steel," Thesis submitted in partial fulfillment for the Sc D degree in Metallurgy at the Massachusetts Institute of Technology, June 1960.

8. J. Neill Greenwood, "The Influence of Vibration on the Creep of Lead." ASTM Proceedings, Vol. 49, pp. 834-850, (1949)

9. L. F. Coffin, Jr., "The Stability of Metals under Cyclic Plastic Strain," Journal of Basic Eng., Trans. ASME, Vol. 82, Ser. D. No. 3, p. 671 (1960).

10. G. J. Moyar, "A Mechanics Analysis of Rolling Element Failures," Dept. of Theoretical and Applied Mechanics Report No. 182, University of Illinois, Dec. 1960, p. 55.

11. H. M. Bendler and W. A. Wood, "Effect of Superimposed Static Tension on the Fatigue Process on Copper Subjected to Alternating Torsion," Trans. of Metallurgical Society of AIME, Feb. 1962, p. 18.

12. G. J. Moyar and G. M. Sinclair, authors' closure to discussion of "Cumulative Plastic Deformation in Rolling Contact," ASME paper No. 62-Met-4 (1962).

13. J. D. Lubahn and R. P. Felgar, Plasticity and Creep of Metals, John Wiley and Sons, Inc., New York, 1961, p. 495.

14. A. E. Johnson, J. Henderson and V. Mathur, "Creep under Changing Complex Stress Systems," Engineer, Vol. 206, pp. 209-216; 251-260; 287-291, (1958).

15. A. E. Johnson, "Complex-Stress Creep of Metals," Metallurgical Reviews, published by the Inst. of Metals, Vol. 5, No. 20, pp. 447-506, (1960).

16. G. I. Taylor and H. Quinney, "The Plastic Deformation of Metals," Philosophical Transactions of the Royal Society, Ser. A. Vol. 230, pp. 323-362, (1931-32).

17. R. Hill, The Mathematical Theory of Plasticity, Oxford, 1950, p. 72.

18. P. D. Schwiebert and G. J. Moyar, "An Application of Linear Hardening Plasticity Theory to Cycle and Path Dependent Strain Accumulation," Dept. Theoretical and Applied Mechanics Report No. 212, University of Illinois, Jan. 1962.

19. W. A. Backofen, A. J. Shaler and B. B. Hundy, "Mechanical Anisotrophy in Copper," Trans. Amer. Soc. for Metals, Vol. 45, pp. 655-680 (1954)

20. J. Parker and J. Kettlewell, "Plastic Stress-Strain Relationship - Further Experiments on the Effect of Loading History," Journal of Applied Mechanics, Sept. 1961, pp. 439-446.

TABLE I

Specimen Number	Axial Stress	Shear Strain Range	Maximum Shear Stress Range	Minimum Plastic Shear Strain Range	Work/cycle Index	Minimum Cyclic Creep Rate	True Fracture Strain $(\ln l_f/l_o)$	Cycles to Fracture	Fracture Type	Notes
	σ_o psi	$\Delta\gamma_o$ in/in	$2\tau_{max.}$ psi	$\Delta\gamma_{p_{min}}$ in/in	W in-lbs./in^3	$\Delta\epsilon_n$ in/in / 10^7cycles	ϵ_f in/in	N_f		
3-s	11,000	0.0148	29,000	0.0092	276	4640.0	0.306	509	Neck	Dimen. Inst. after N = 160
2-s	7,000	0.0144	27,200	0.0092	260	1610.0	0.247	968	Split	Dimen. Inst. after N = 630
5-s	4,500	0.0145	22,900	0.0098	228	881.0	0.259	2,141	Split	Dimen. Inst. after N = 1,350
4-s	2,000	0.0147	20,100	0.0103	210	407.0	0.141	2,802	Split	
6-s	11,000	0.0115	27,100	0.0062	166	1600.0	0.315	1,685	Neck-split	Dimen. Inst. after N = 440
8-s	7,000	0.0116	23,300	0.0066	163	568.0	0.262	2,871	Split	Dimen. Inst. after N = 1,460
9-s	4,500	0.0108	21,400	0.0068	145	327.0	0.178	2,922	Split	
7-s	2,000	0.0112	19,000	0.0070	130	140.0	0.097	5,206	Split	
24-s	11,000	0.0091	23,900	0.0045	114	670.0	0.234	1,336	Split	Dimen. Inst. after N = 900
23-s	7,000	0.0092	22,200	0.0049	110	239.0	0.251	5,722	Neck-split	Dimen. Inst. after N = 3,400
22-s	4,500	0.0094	20,800	0.0051	110	182.0	0.140	4,078	Split	Failure at grip
15-s	2,000	0.0093	19,000	0.0058	106	58.0	0.074	8,523	Split	
18-s	11,000	0.0069	20,900	0.0032	67	245.0	0.256	5,045	Neck-split	Dimen. Inst. after N = 2,400
17-s	7,000	0.0072	19,400	0.0035	68	80.0	0.193	9,661	Split	
20-s	4,500	0.0073	18,200	0.0036	67	53.8	0.146	13,477	Split	
14-s	2,000	0.0072	15,400	0.0038	58	19.0	0.053	17,787	Split	
19-s	11,000	0.0053	17,000	0.0019	35	49.6	0.174	10,073	Split	
10-s	7,000	0.0056	16,300	0.0021	34	27.2	0.114	15,418	Split	
21-s	4,500	0.0055	14,000	0.0026	38	15.1	0.069	21,277	Split	
13-s	2,000	0.0057	12,300	0.0030	36	4.8	0.033	38,950	Split	

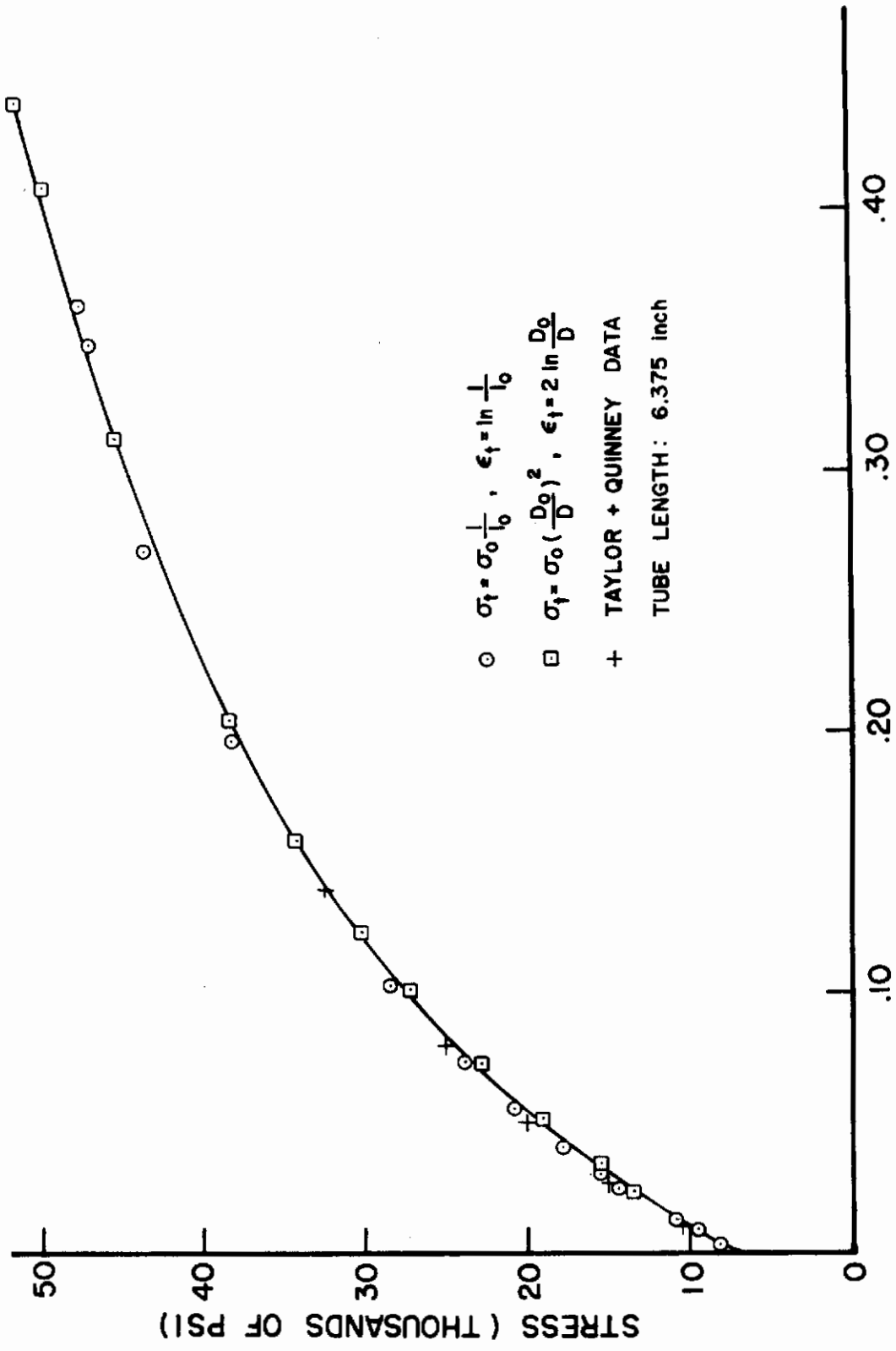

Fig. 1 TRUE STRESS-STRAIN CURVE FOR ANNEALED OFHC COPPER TUBING

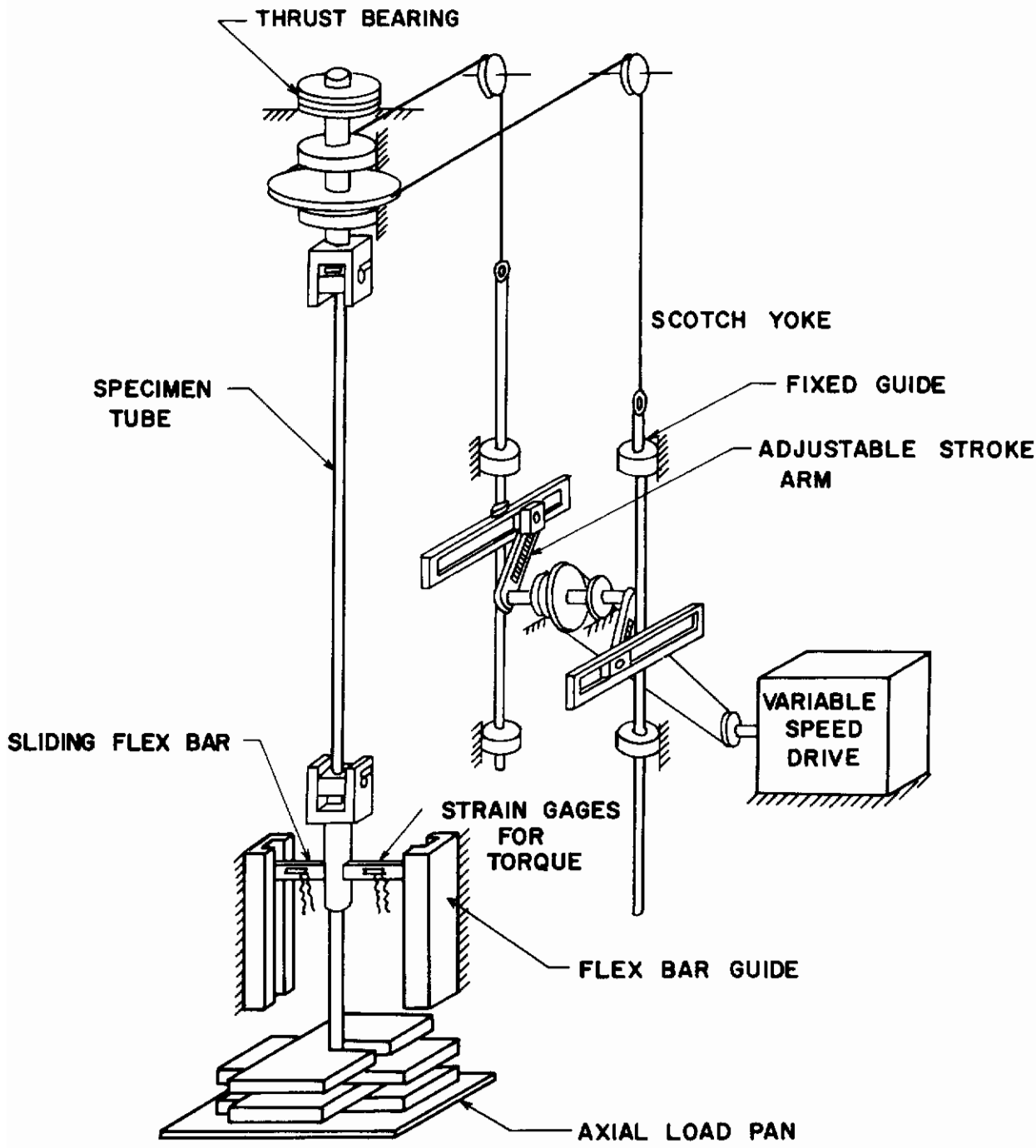

FIG. 2 SCHEMATIC DIAGRAM OF APPARATUS

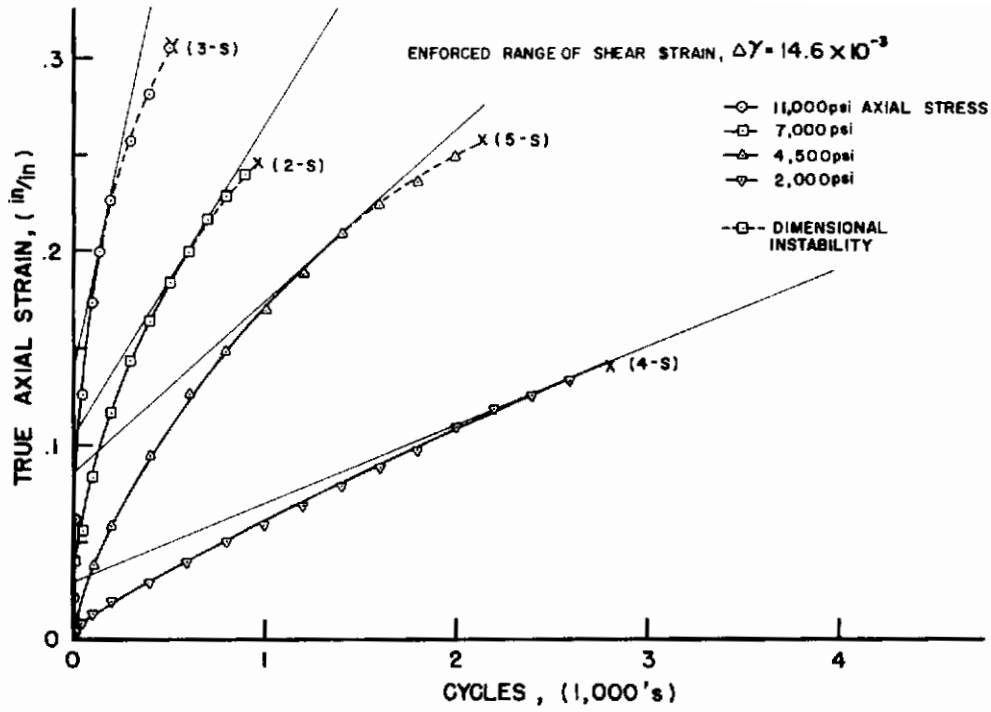

Fig. 3a

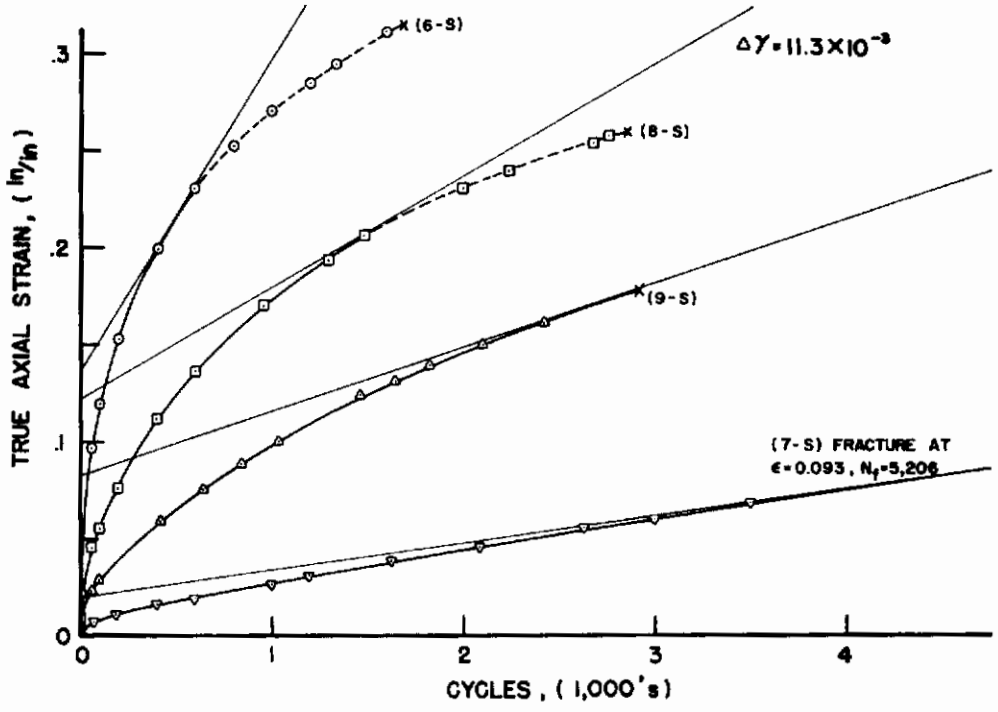

Fig. 3b

Fig. 3 CYCLIC AXIAL STRAIN ACCUMULATION

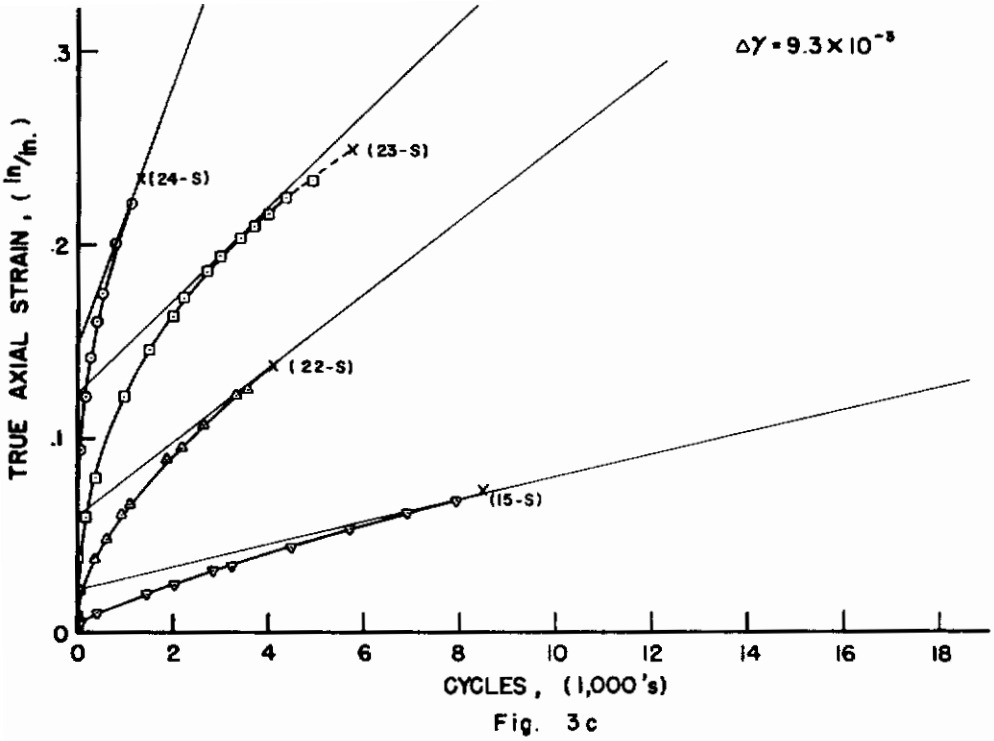

Fig. 3c

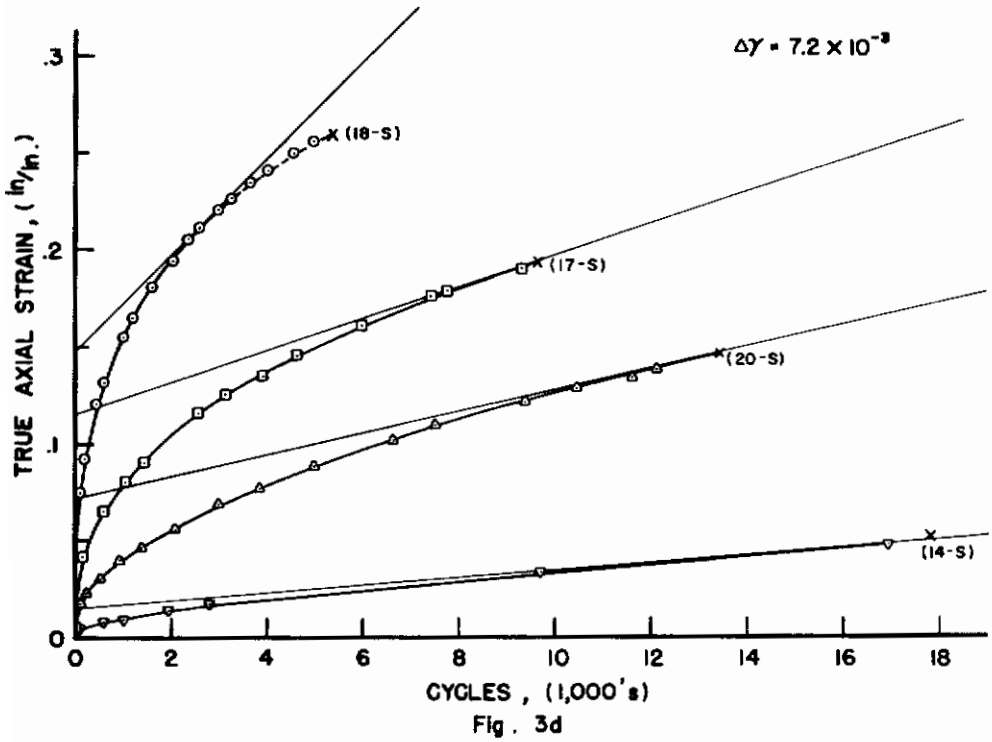

Fig. 3d

Fig. 3 CYCLIC AXIAL STRAIN ACCUMULATION

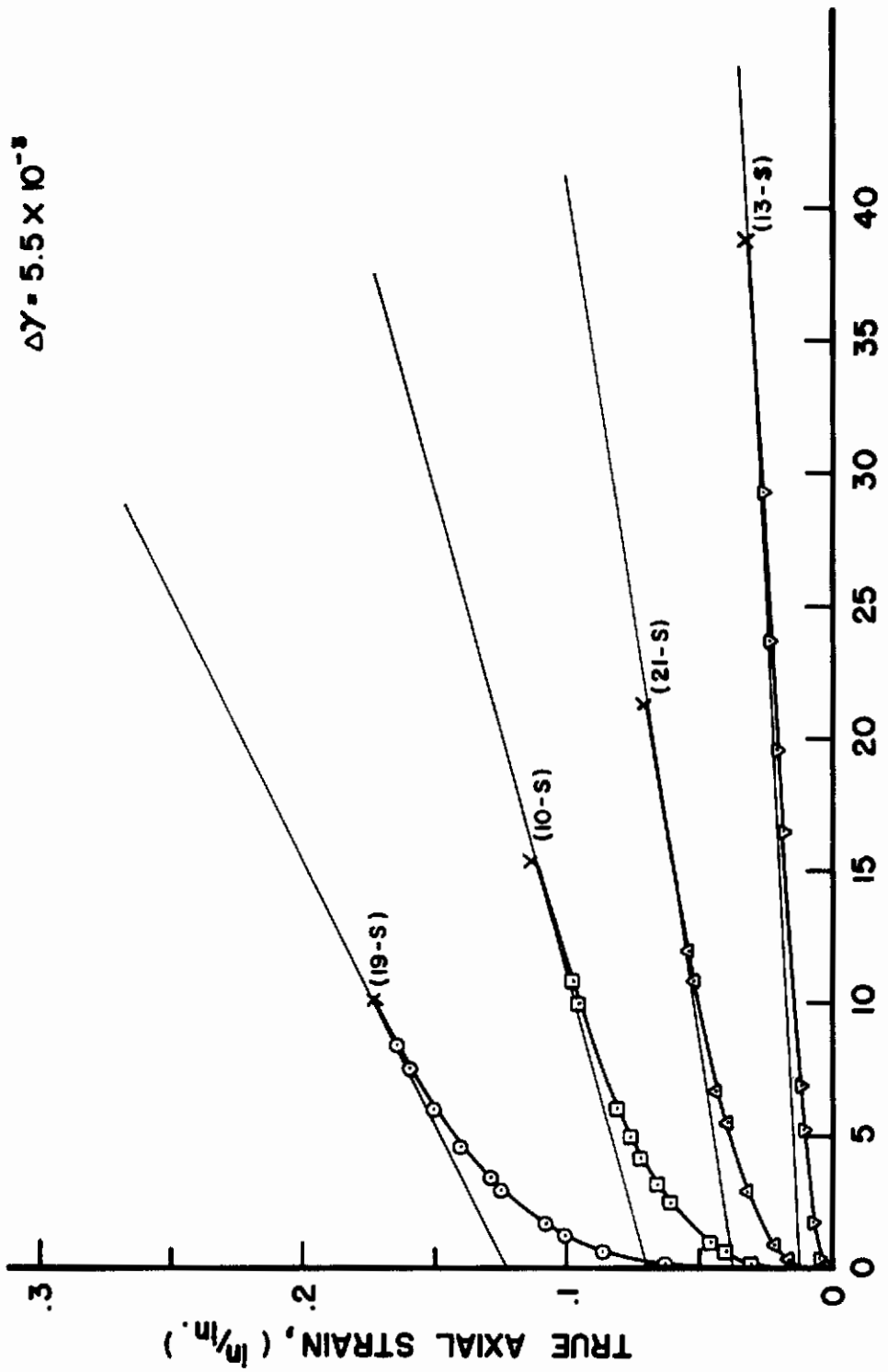

Fig. 3e

Fig. 3 CYCLIC AXIAL STRAIN ACCUMULATION

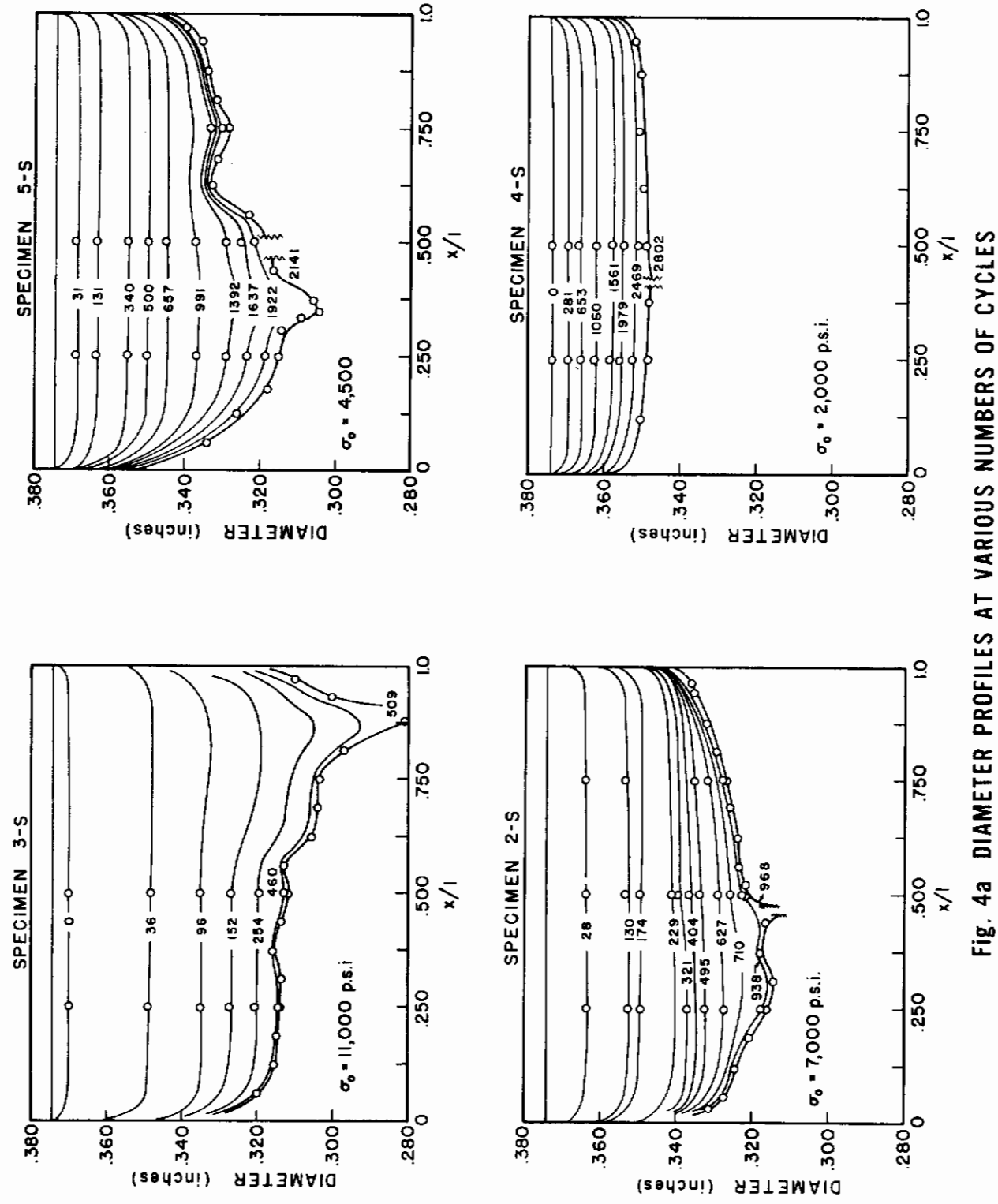

Fig. 4a DIAMETER PROFILES AT VARIOUS NUMBERS OF CYCLES

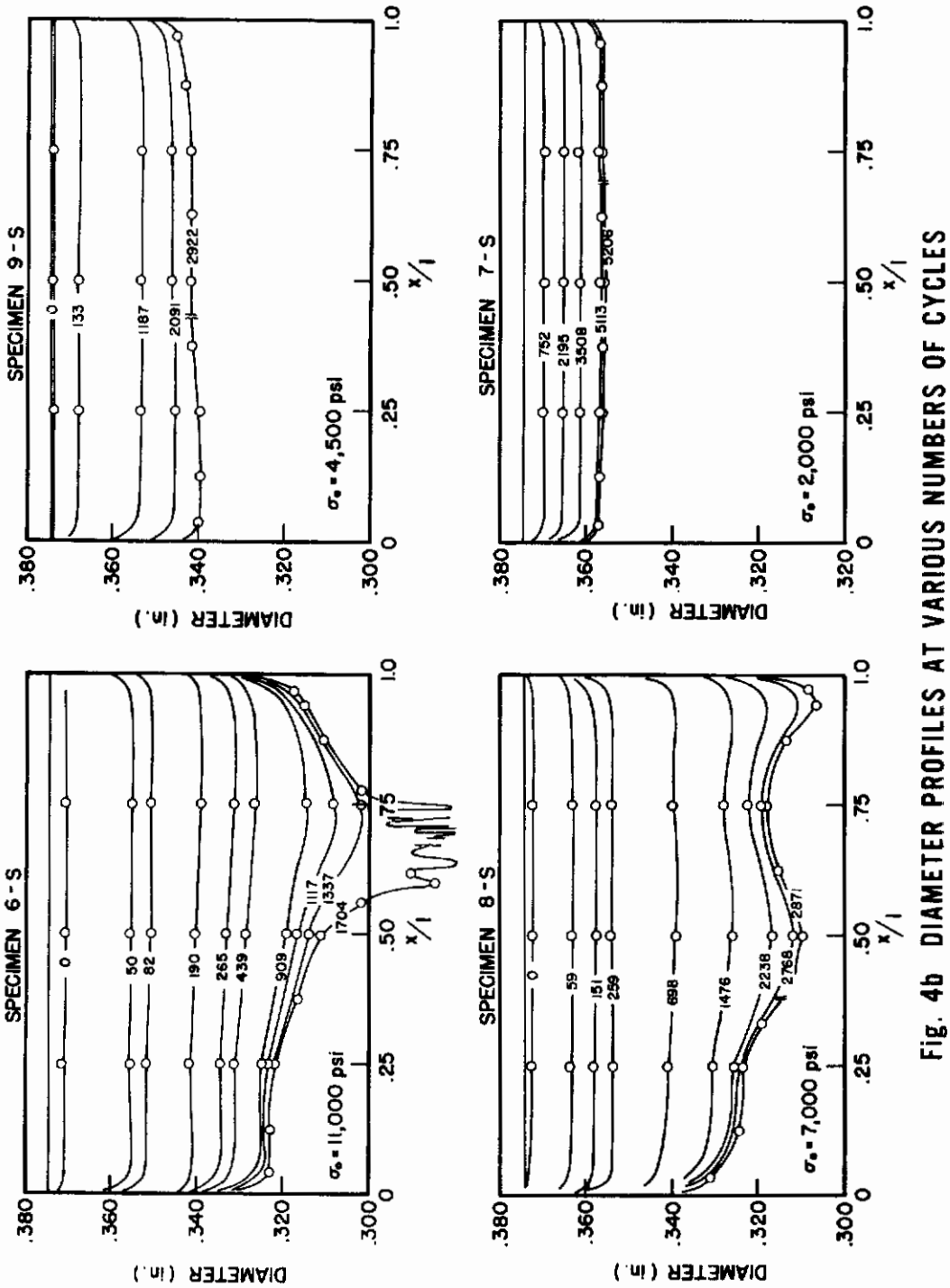

Fig. 4b DIAMETER PROFILES AT VARIOUS NUMBERS OF CYCLES

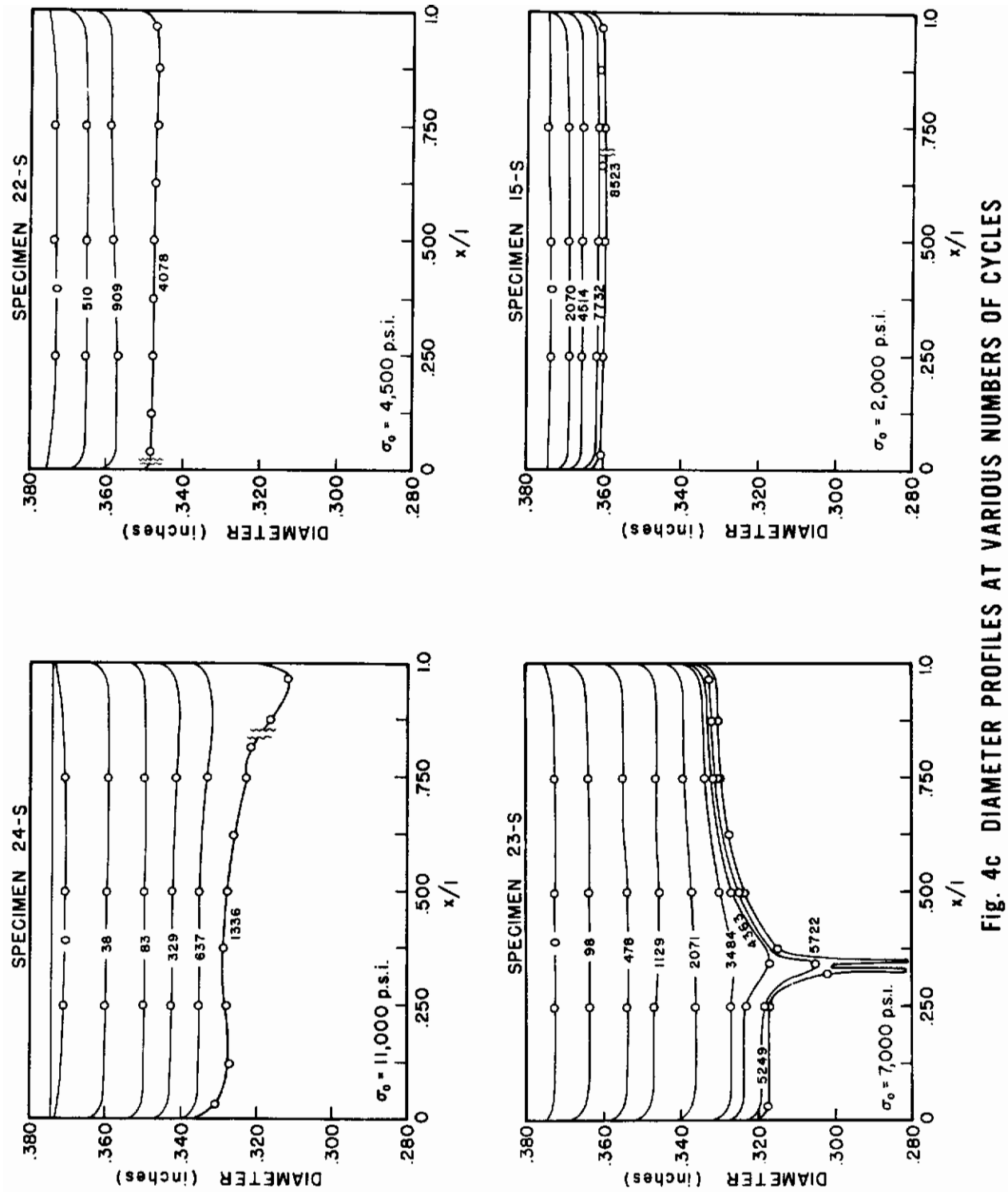

Fig. 4c DIAMETER PROFILES AT VARIOUS NUMBERS OF CYCLES

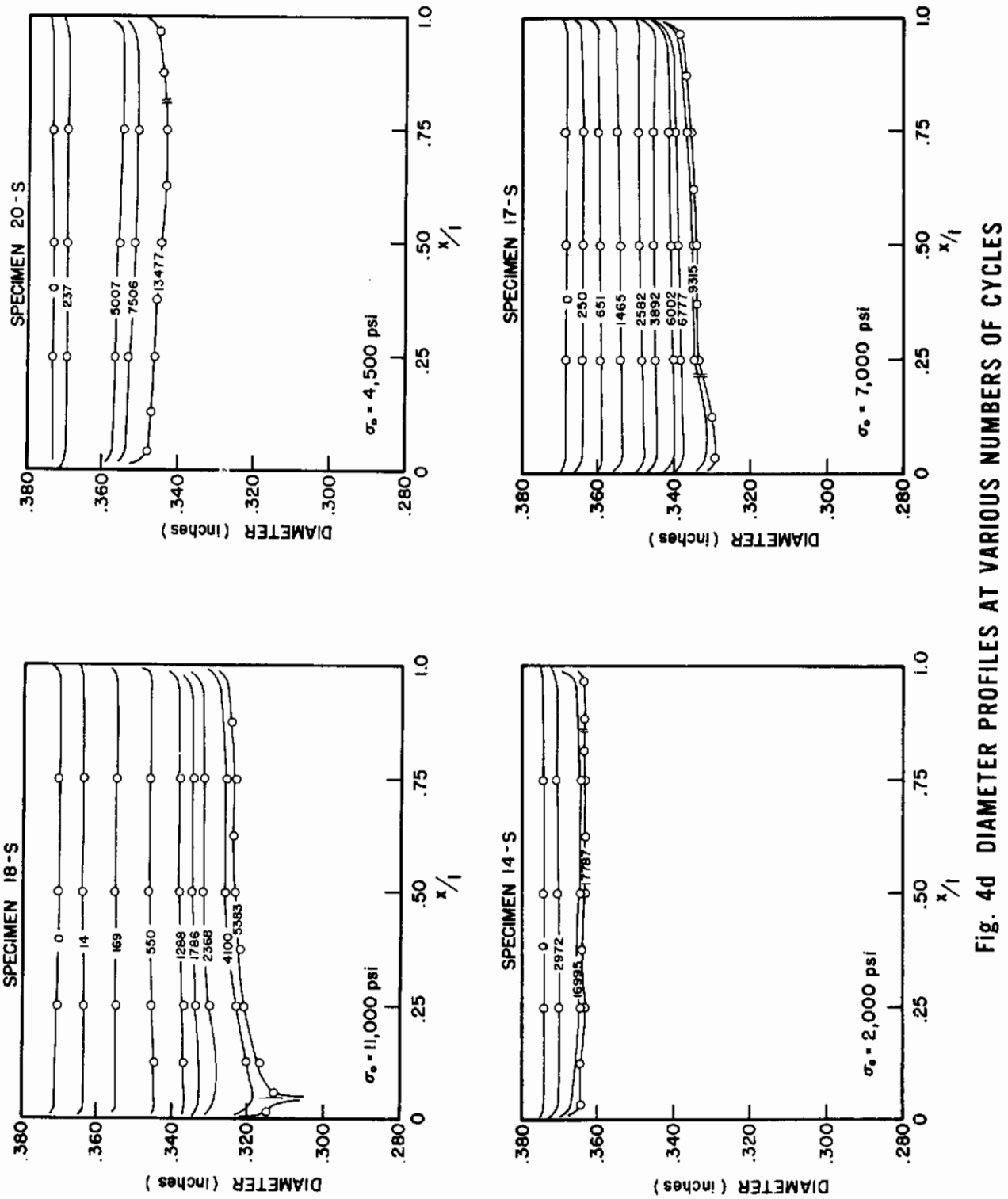

Fig. 4d DIAMETER PROFILES AT VARIOUS NUMBERS OF CYCLES

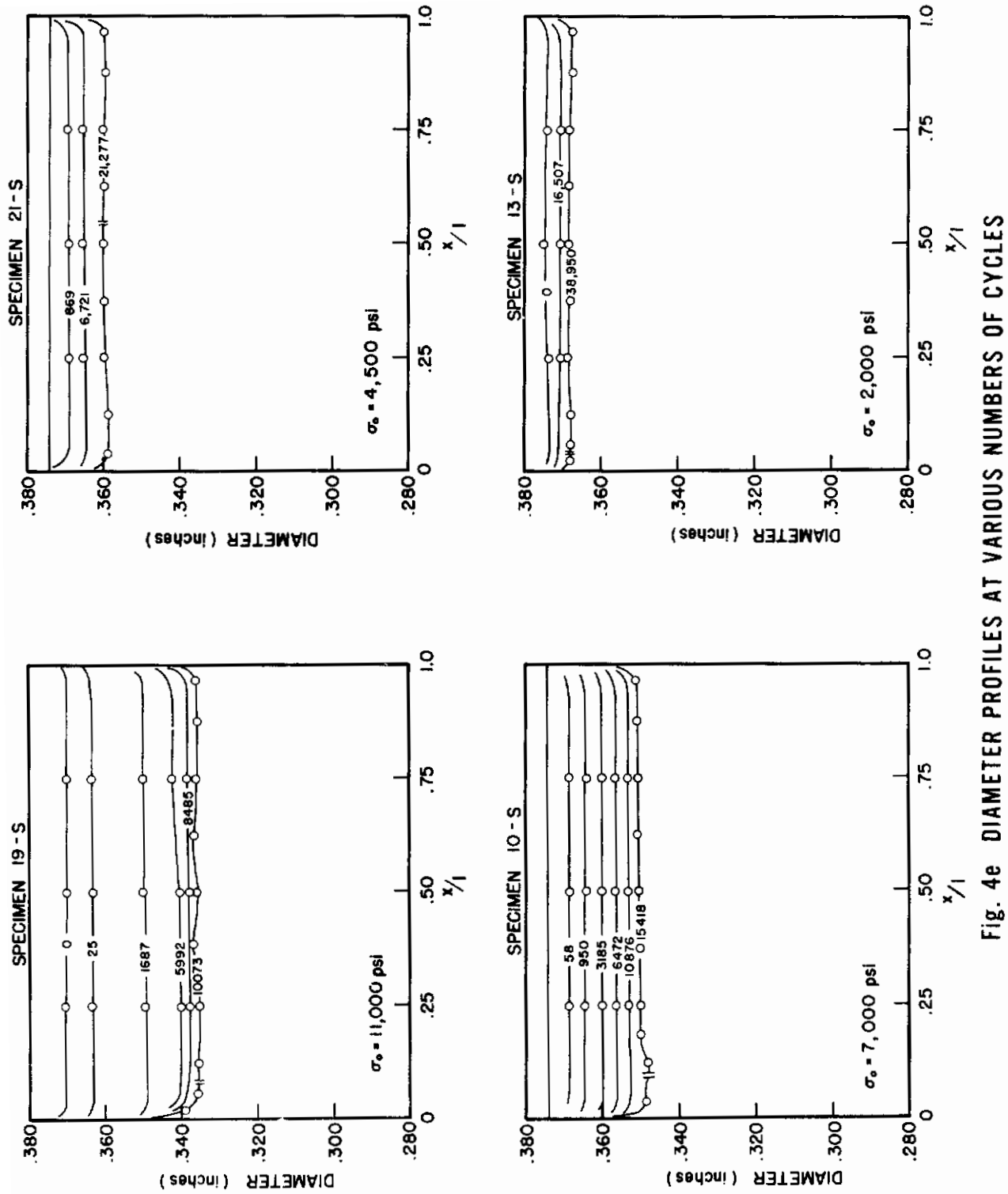

Fig. 4e DIAMETER PROFILES AT VARIOUS NUMBERS OF CYCLES

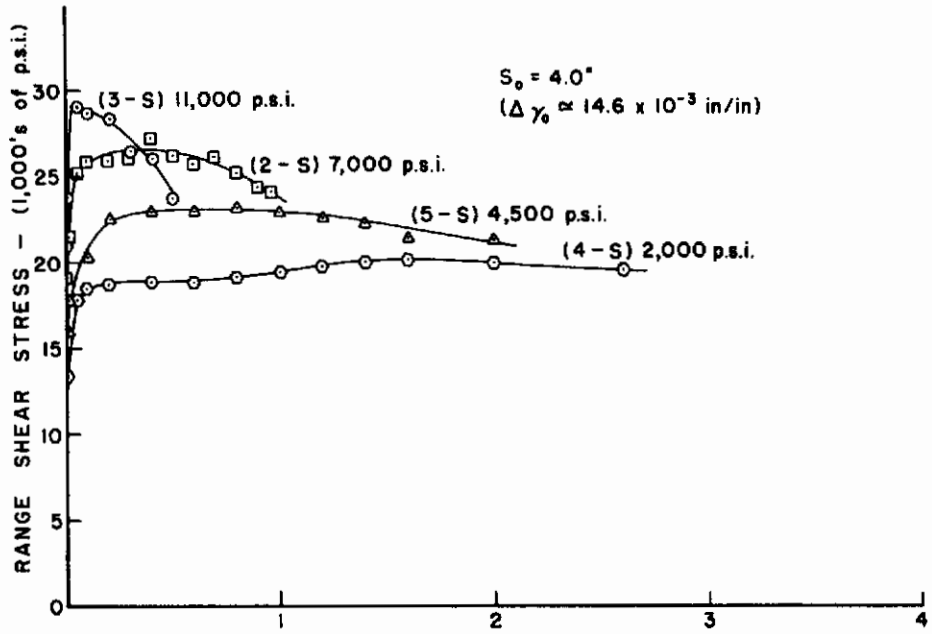

Fig. 5a

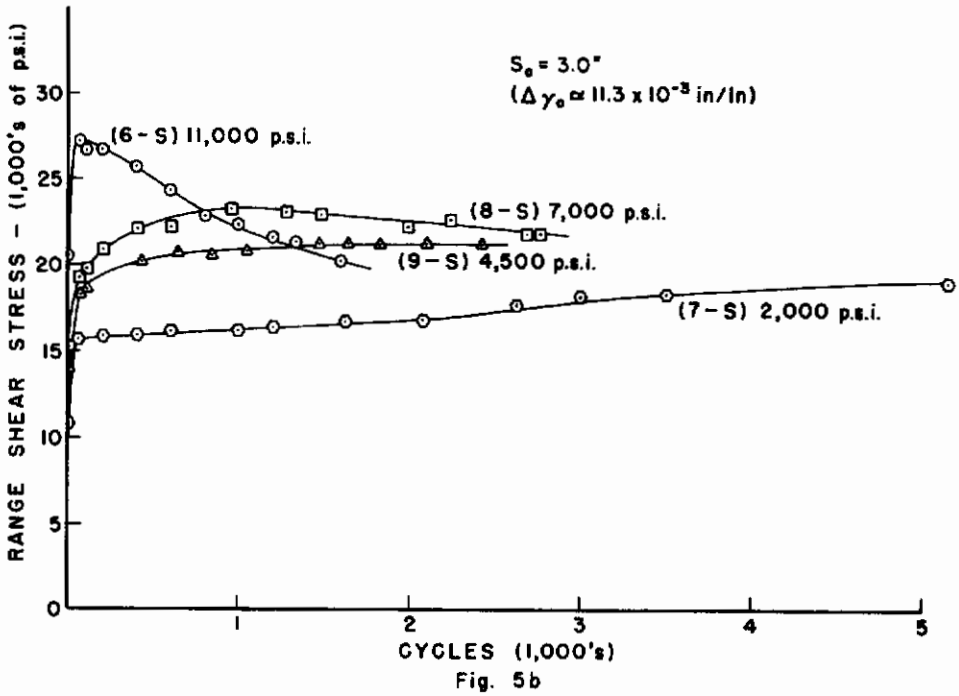

Fig. 5b

Fig. 5 CYCLIC CHANGE IN RANGE OF SHEAR STRESS

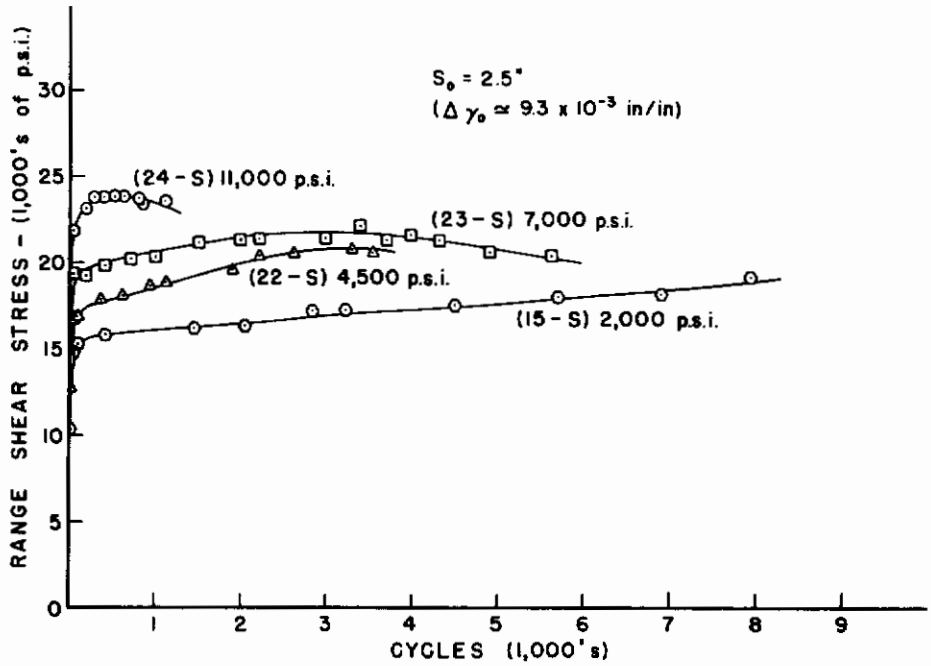

Fig. 5c

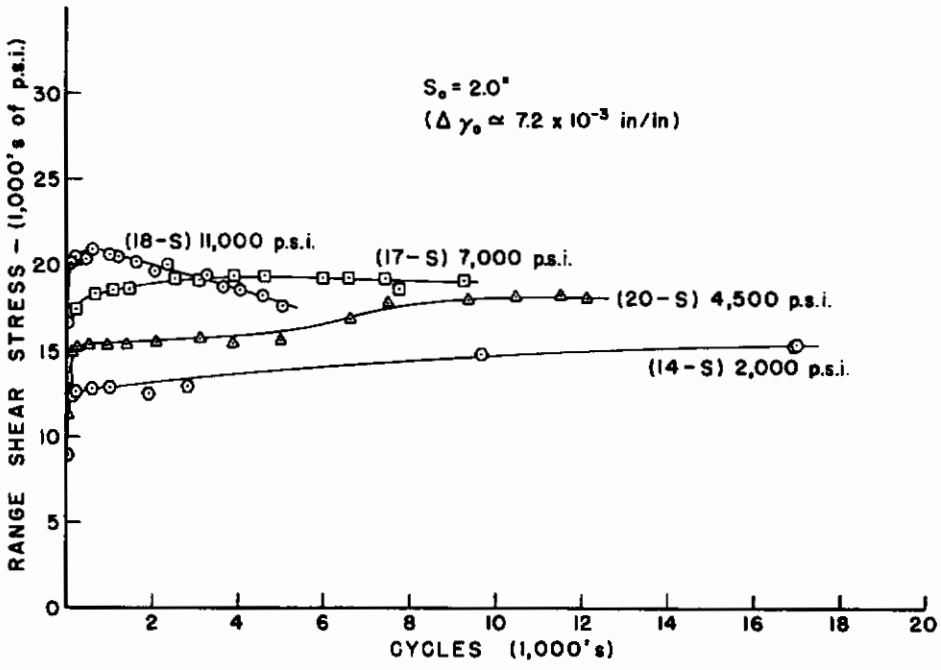

Fig. 5d

Fig. 5 CYCLIC CHANGE IN RANGE OF SHEAR STRESS

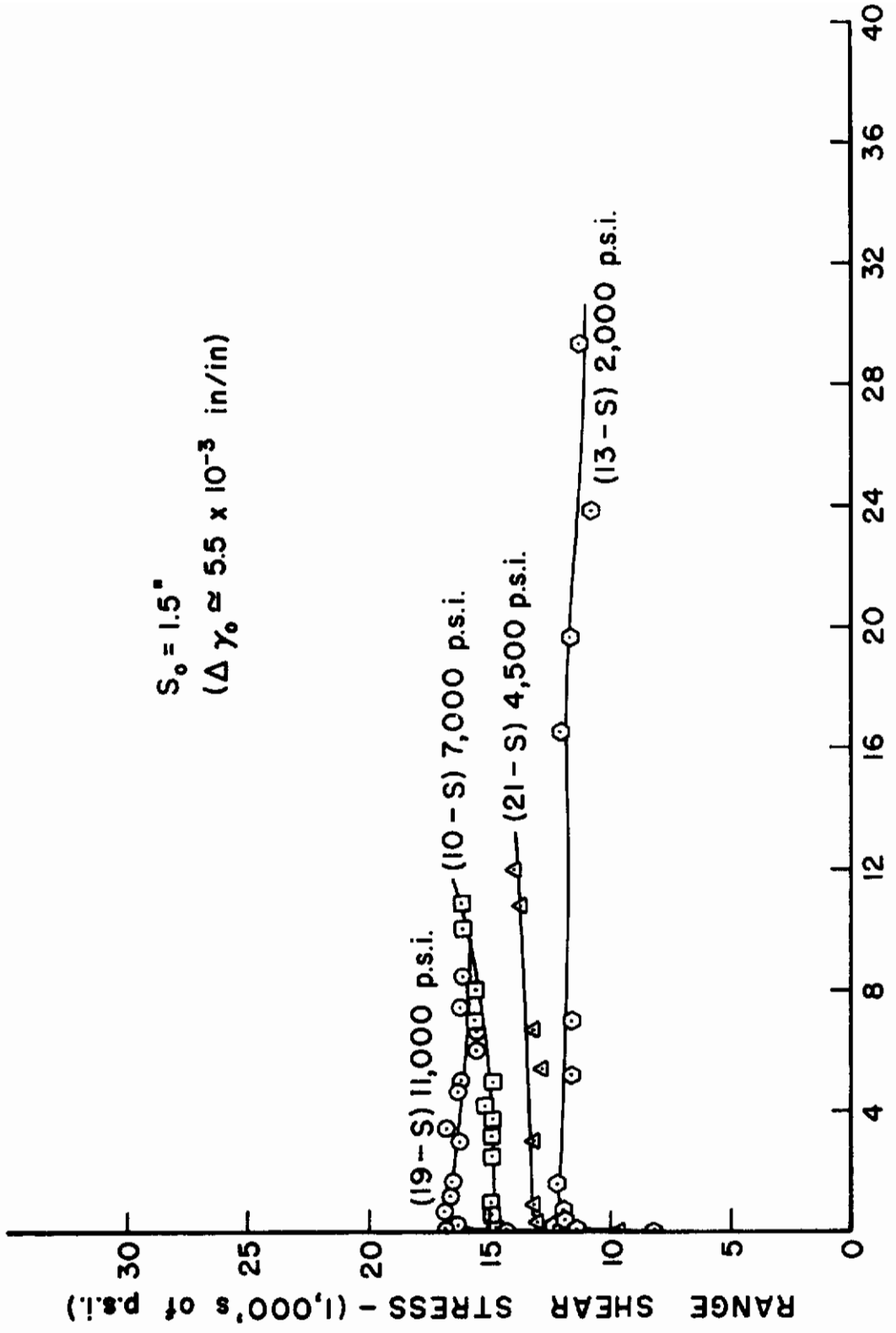

Fig. 5e

Fig. 5 CYCLIC CHANGE IN RANGE OF SHEAR STRESS

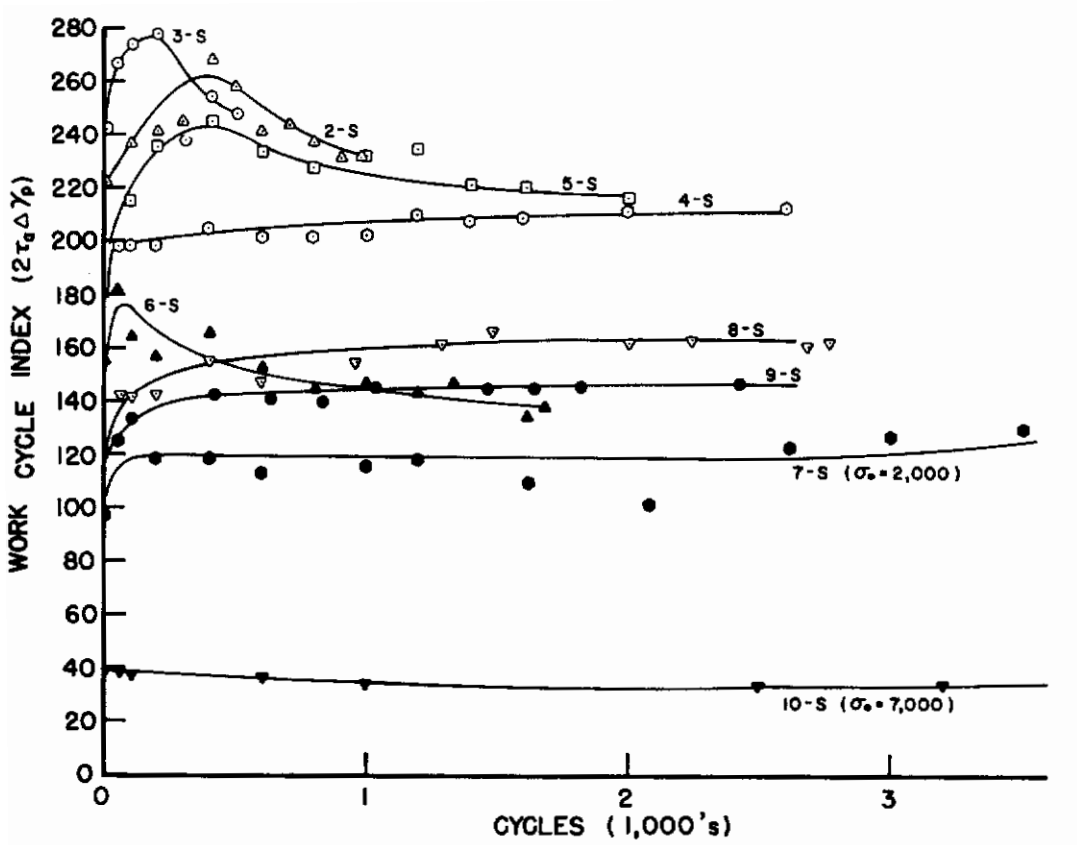

Fig. 6 CYCLIC CHANGE IN WORK INDEX

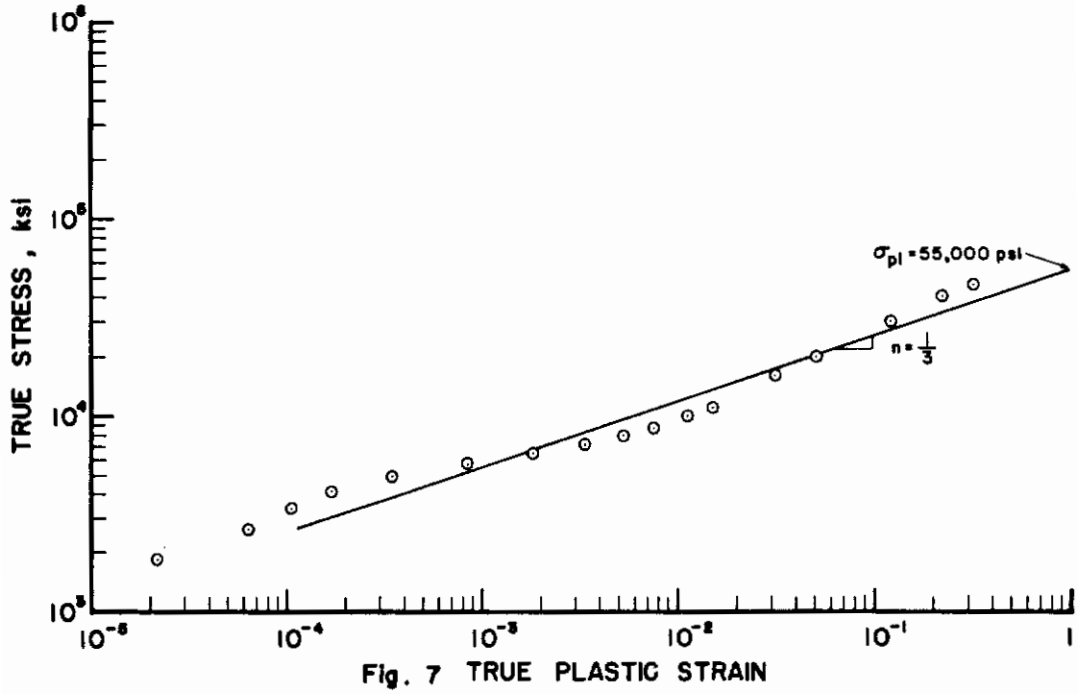

Fig. 7 TRUE PLASTIC STRAIN

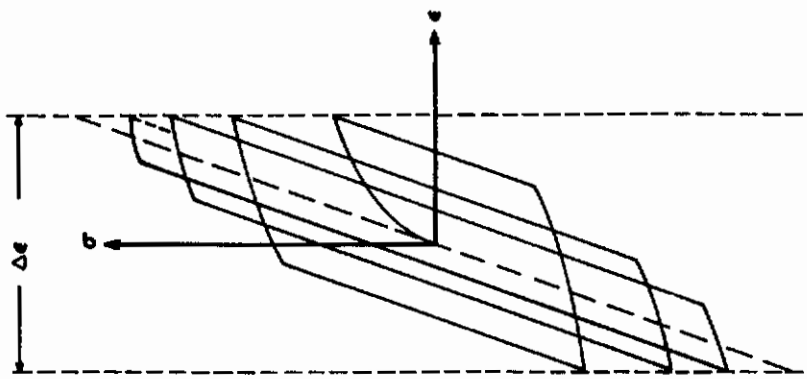

Fig. 9 ONE DIMENSIONAL ISOTROPIC HARDENING MODEL UNDER ALTERNATING STRAIN

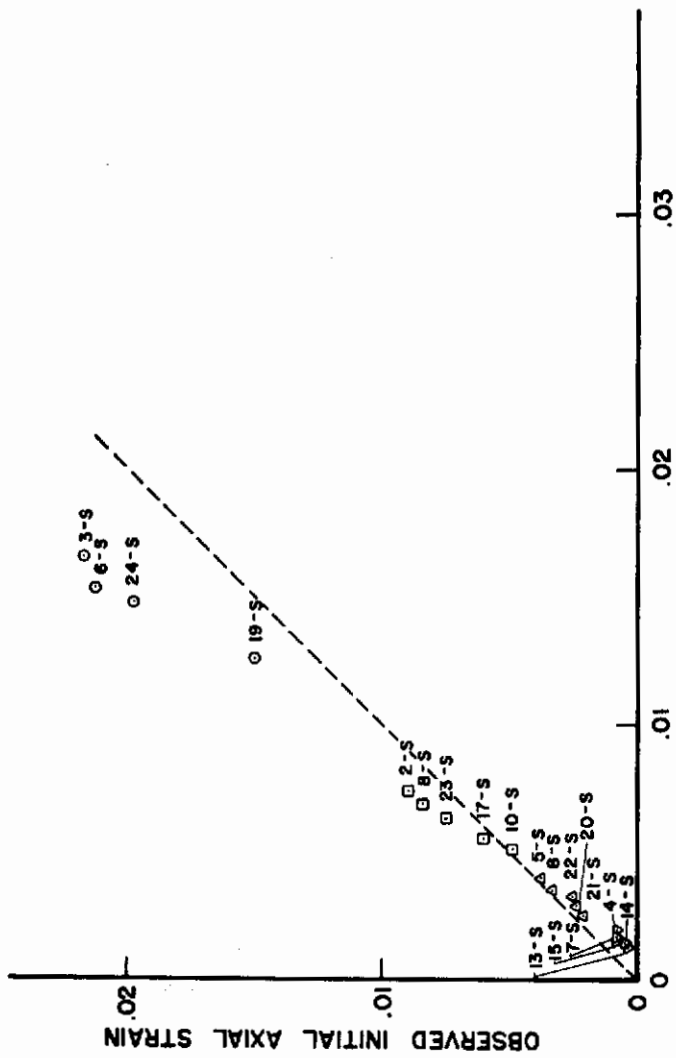

Fig. 8 COMPARISON OF OBSERVED AND THEORETICAL VALUES OF AXIAL STRAIN AFTER FIRST APPLICATION OF TWIST

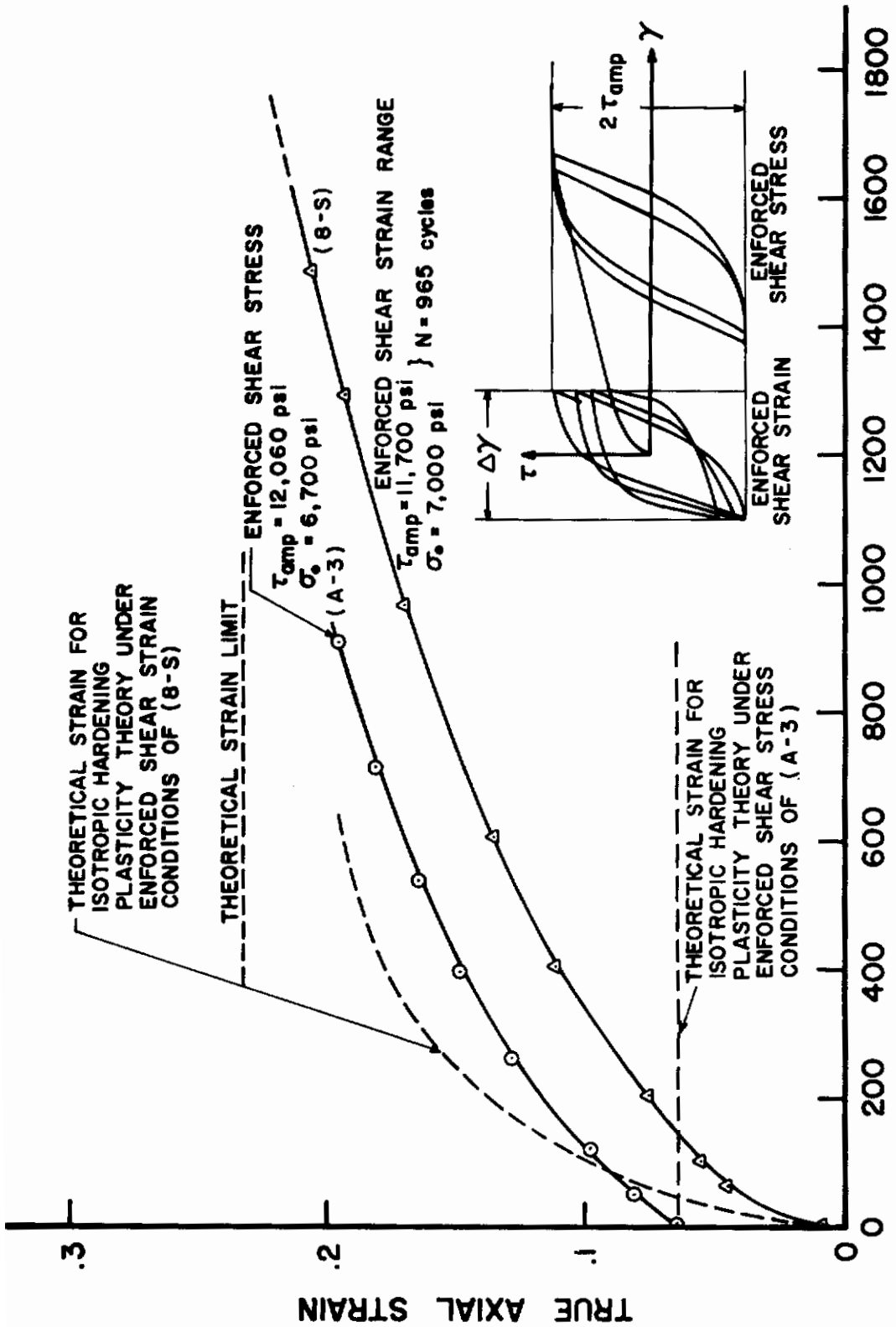

Fig. 10 OBSERVED AND THEORETICAL STRAIN ACCUMULATION FOR CONDITIONS OF ENFORCED SHEAR STRAIN AND ENFORCED SHEAR STRESS

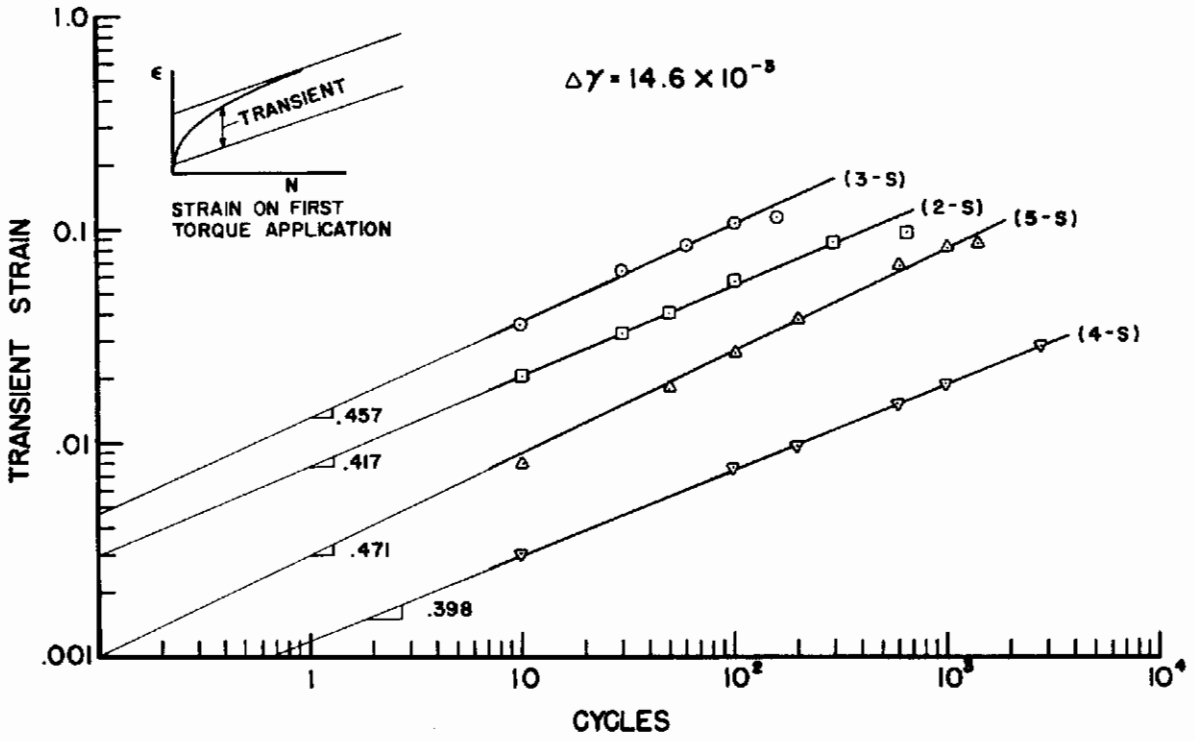

Fig. 11a CYCLIC TRANSIENT STRAIN

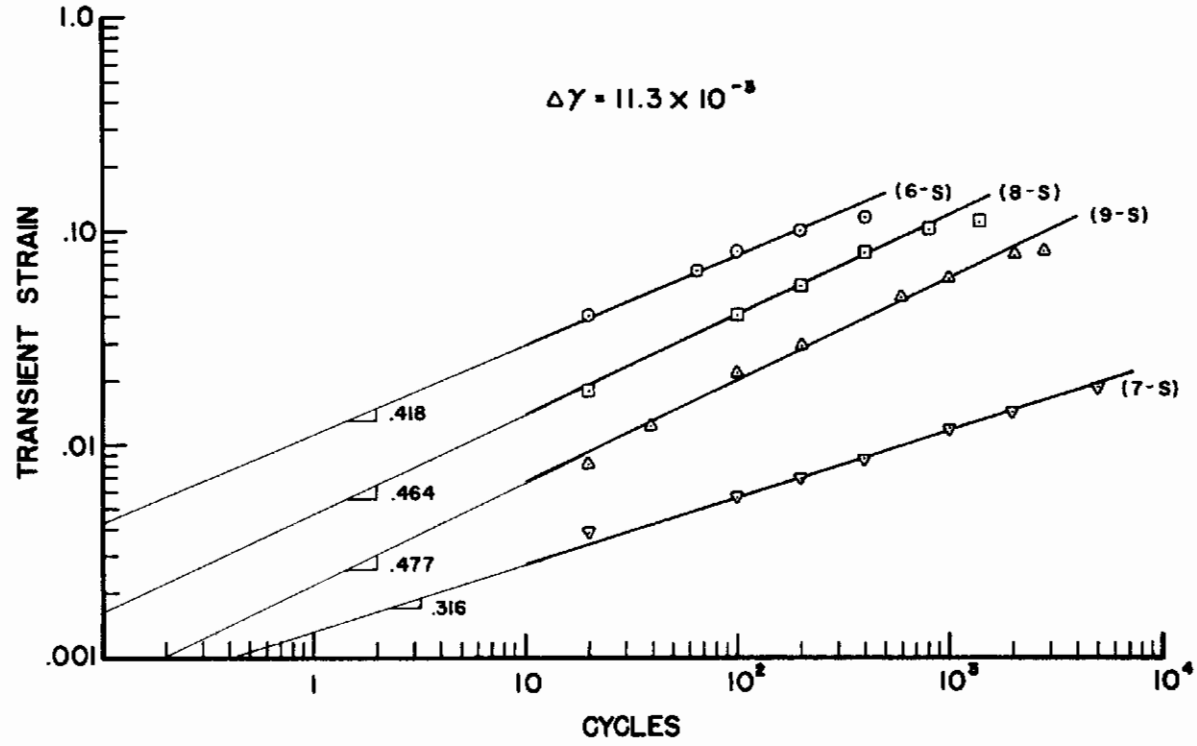

Fig. 11b CYCLIC TRANSIENT STRAIN

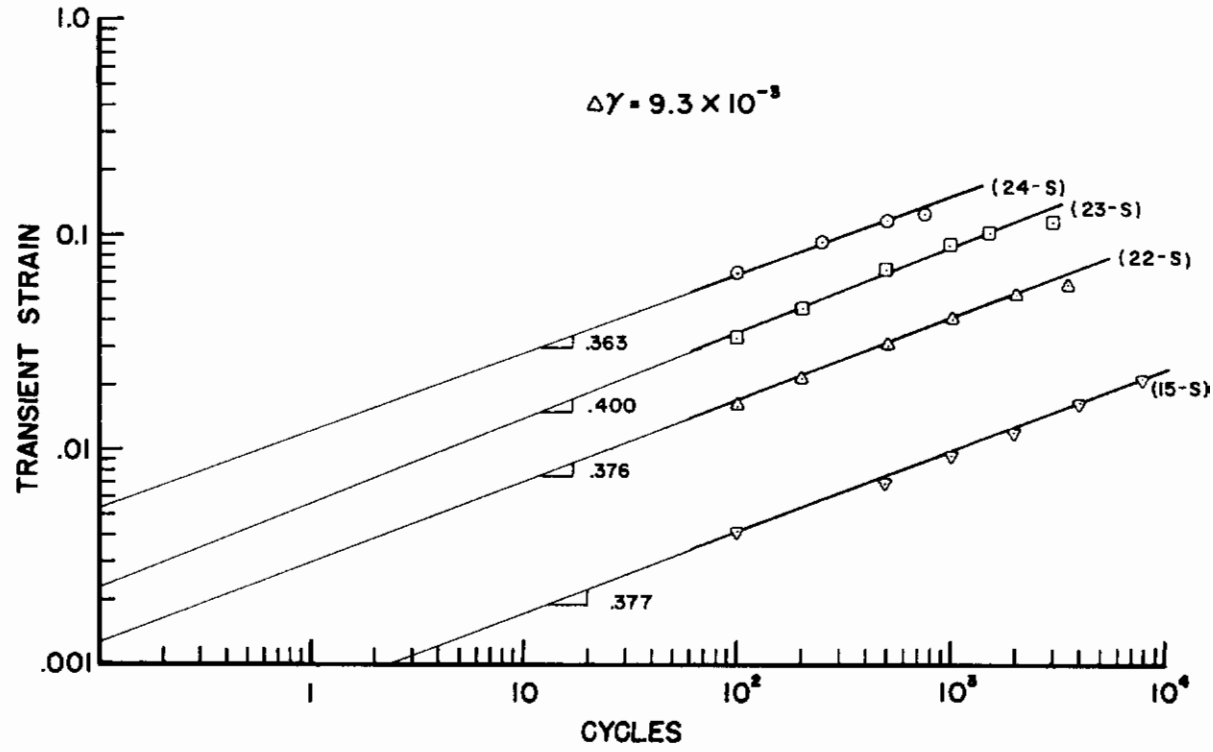

Fig. 11c CYCLIC TRANSIENT STRAIN

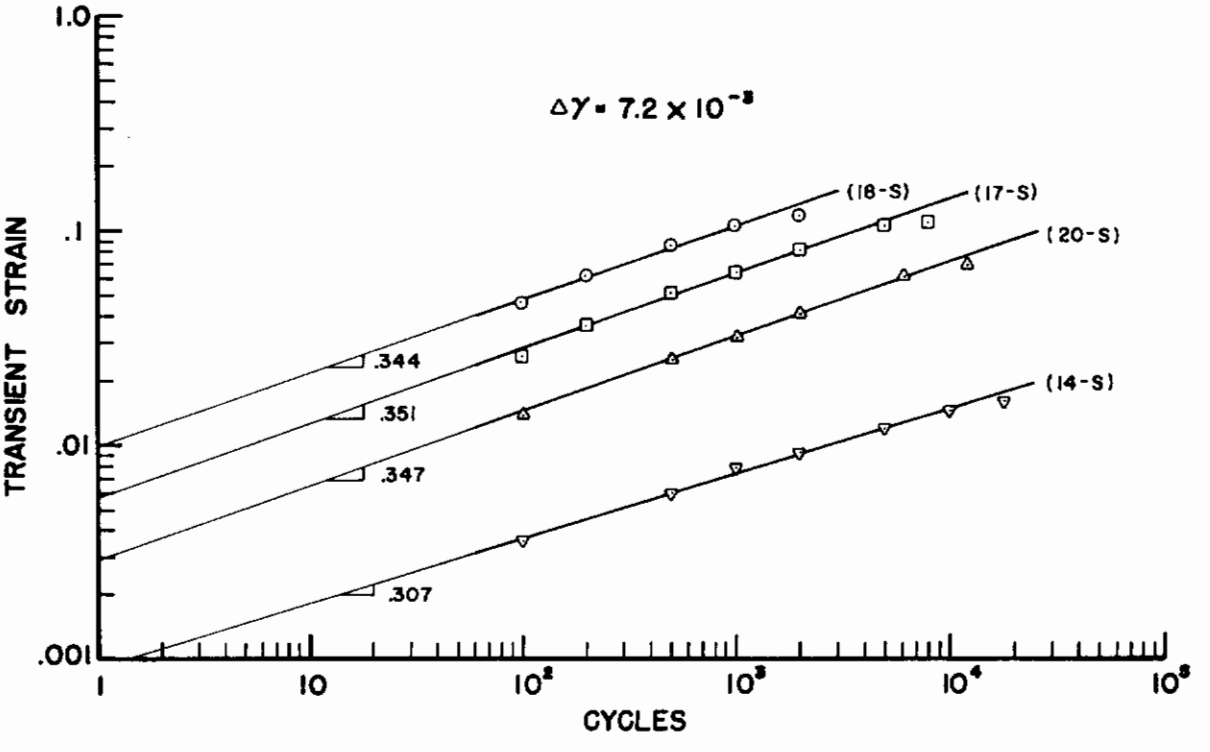

Fig. 11d CYCLIC TRANSIENT STRAIN

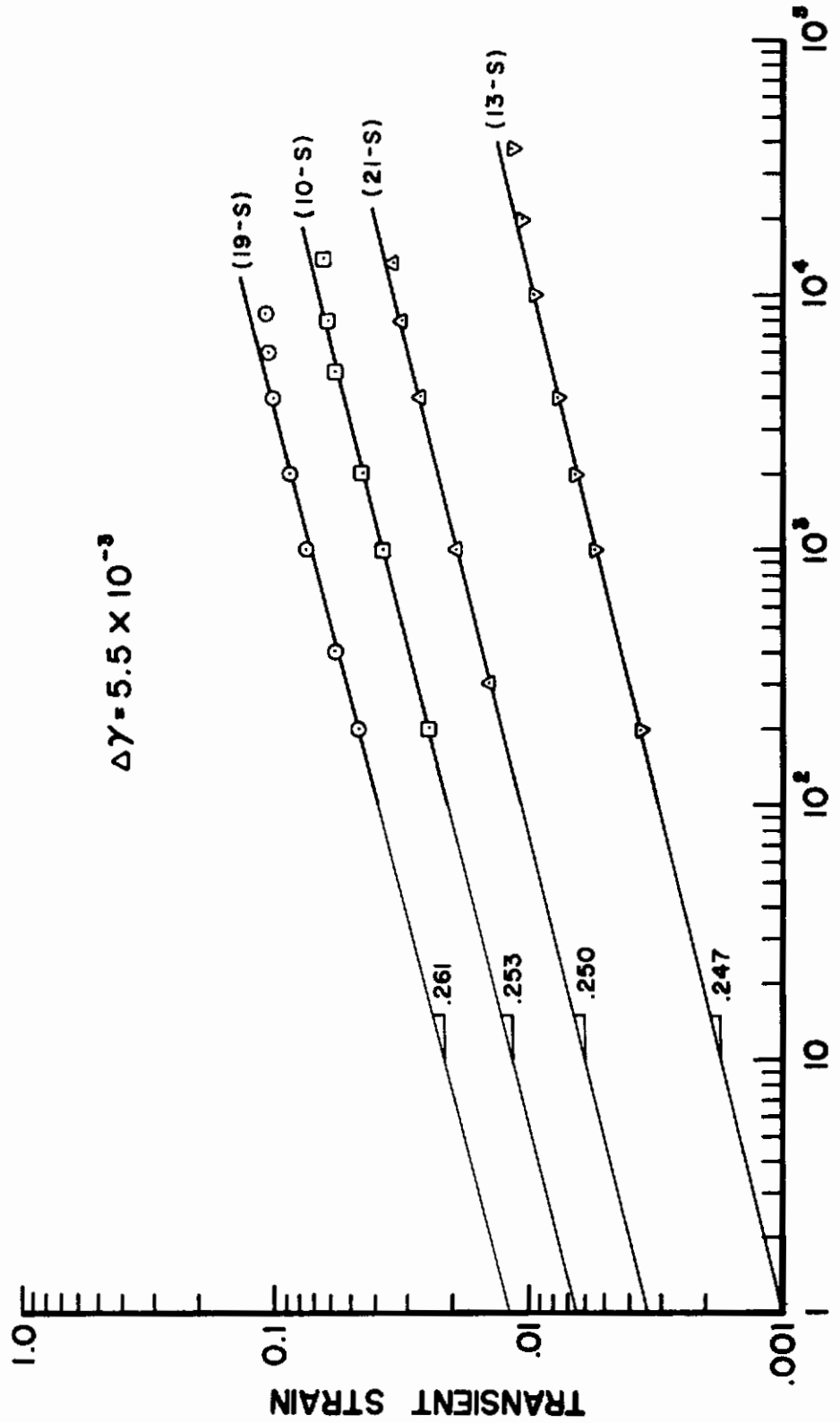

Fig. 11e CYCLIC TRANSIENT STRAIN

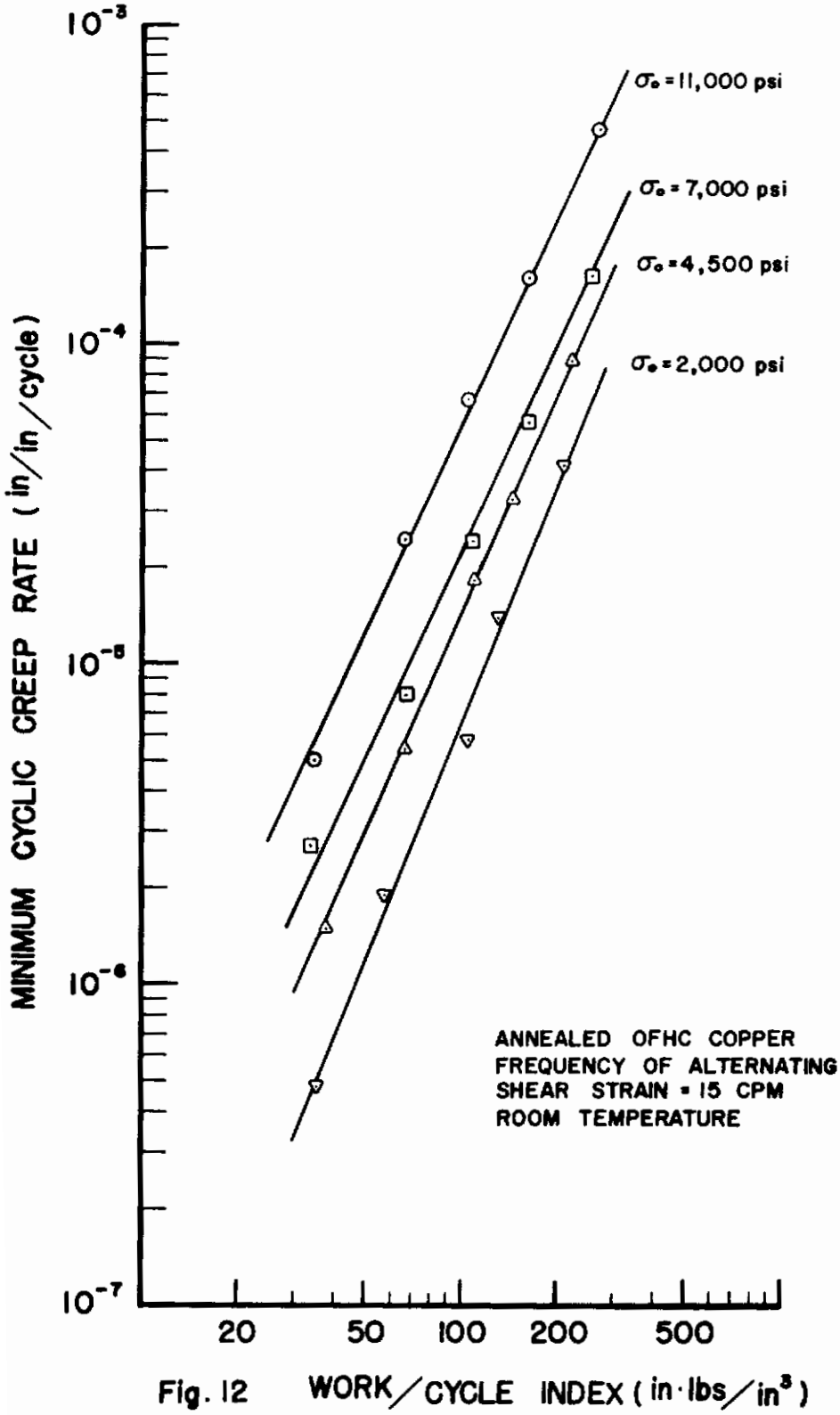

Fig. 12

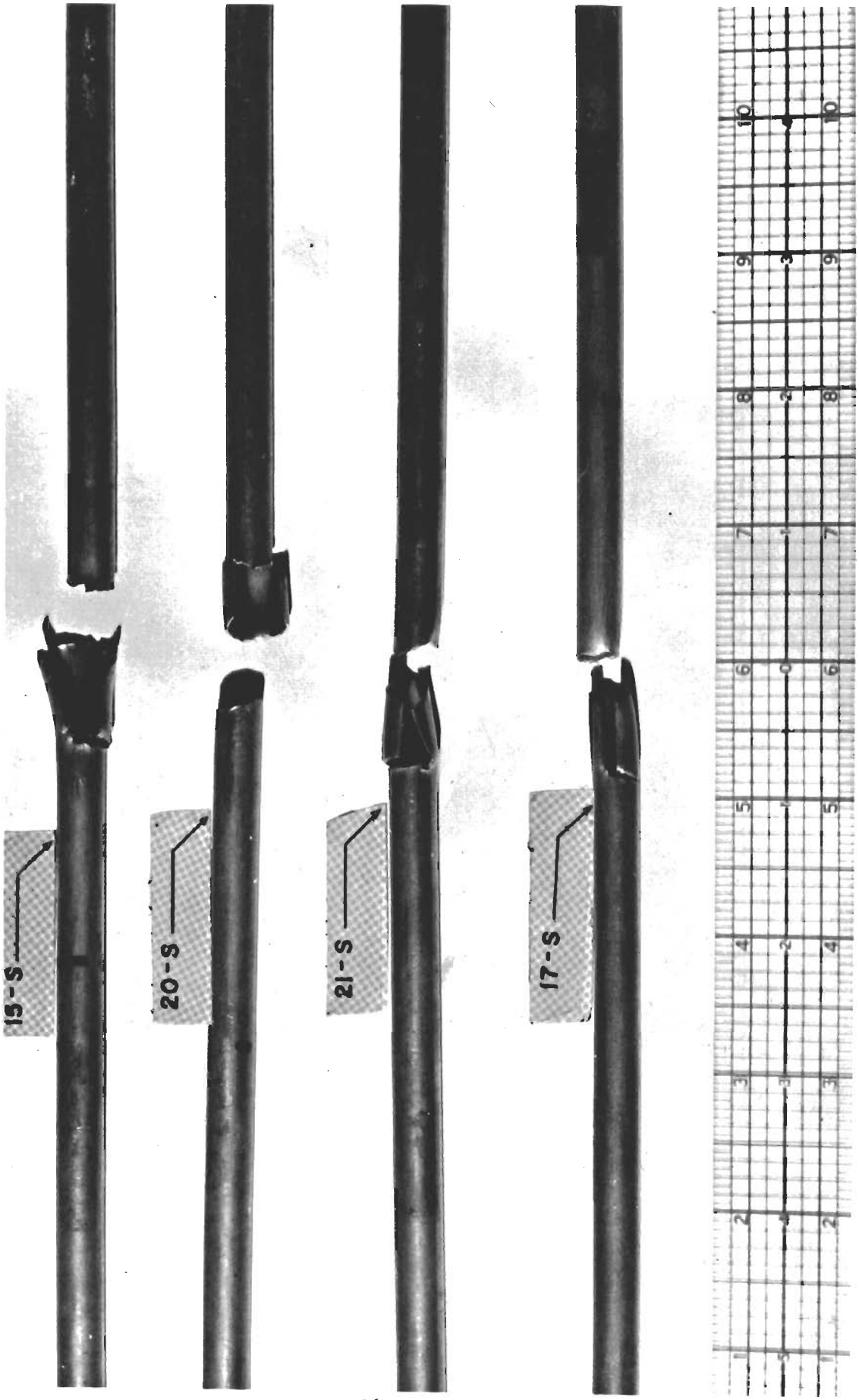

Fig. 13a Typical Fatigue 'Split' Fractures

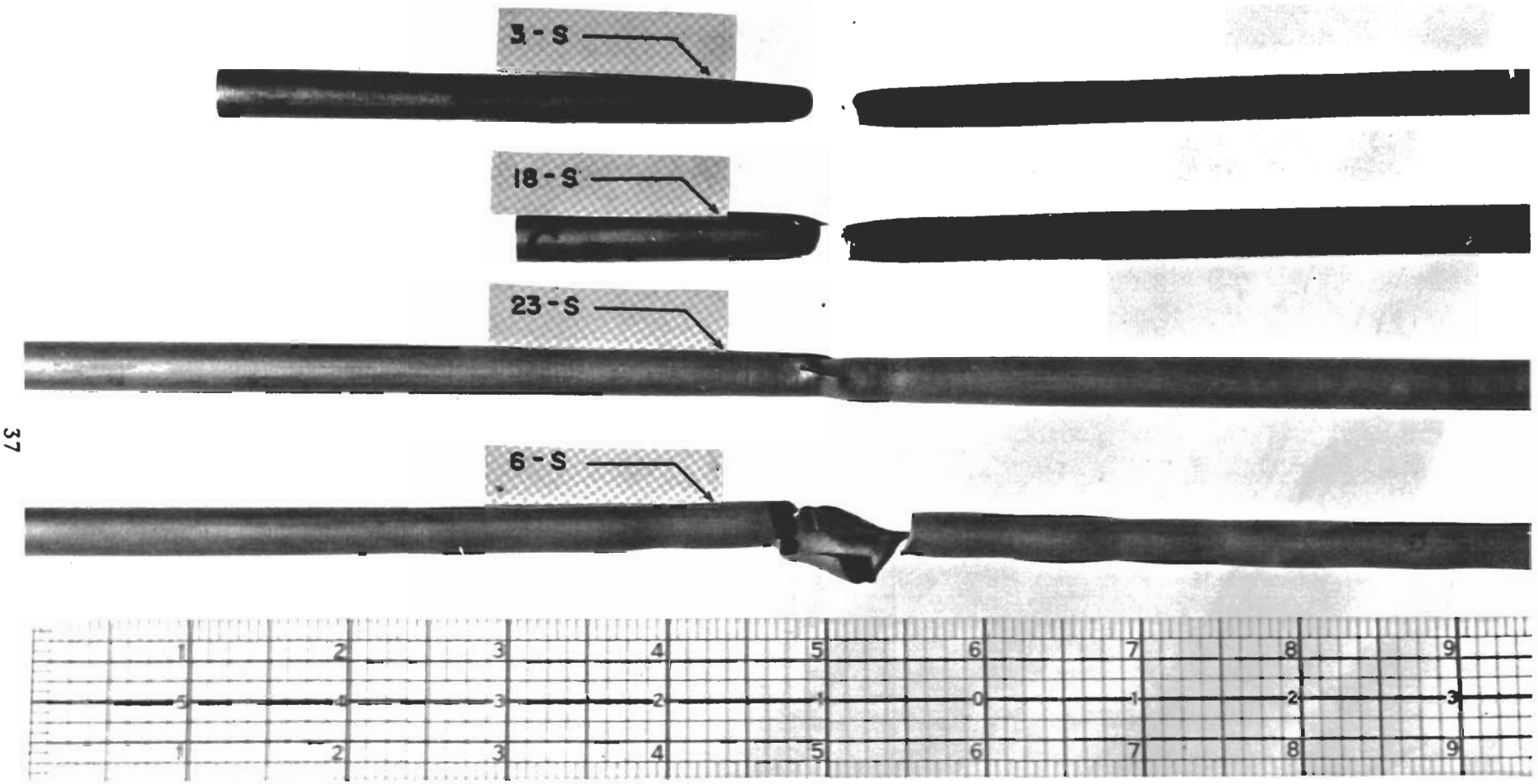

Fig. 13b Fractures with Instability Necking

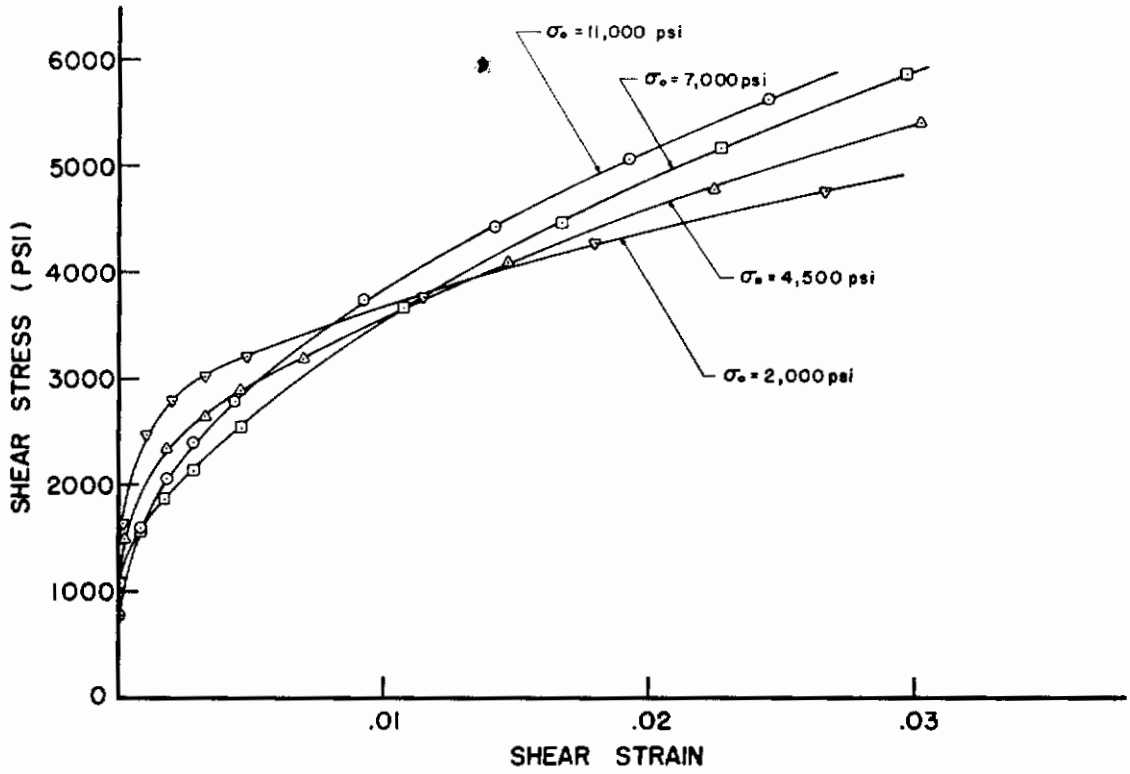

Fig. 14 INFLUENCE OF STEADY AXIAL STRESS ON SHEAR STRESS-STRAIN RELATION FOR MONOTONICALLY INCREASING SHEAR STRAIN

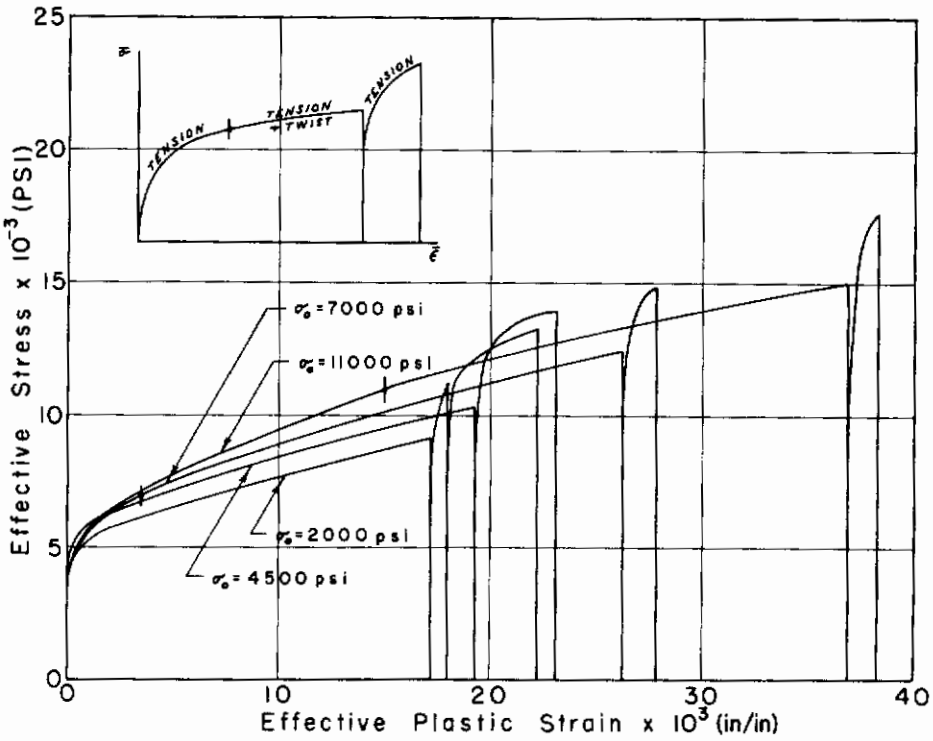

Fig. 15 Summary of Results - Special Initial Loading Conditions.

Appendix

Definition of Terms

A	coefficient in cyclic creep rate equation
B	exponent of W in cyclic creep rate equation
D	current diameter of specimen tube
D_o	original diameter of specimen tube
E	modulus of elasticity
G	modulus of elasticity in shear
H'	slope of effective stress-plastic strain curve
N	number of cycles
W	plastic work/cycle index, product of shear stress range and plastic range of shear strain at steady state condition
ℓ	current length of specimen tube
ℓ_o	original length of specimen tube
m	number of twist reversals
n	strain hardening exponent
x	variable of integration defined in Eq (7)
y	variable of integration defined in Eq (7)
γ	true shear strain
γ_p	true plastic shear strain
γ_o	amplitude of inforced shear strain
$\Delta\gamma_o$	enforced range of shear strain
$\Delta\gamma_{P\ min}$	minimum range of plastic shear strain
ϵ	true axial strain
ϵ_p	true plastic axial strain
$\bar{\epsilon}_p$	effective plastic strain
$\Delta\epsilon_N$	minimum cyclic creep rate
σ	true axial stress
σ_o	value of steady axial stress
σ_{pl}	strength coefficient
$\bar{\sigma}$	effective stress